Geomatica 76 (2024) 100020

Contents lists available at ScienceDirect

Geomatica

journal homepage: www.sciencedirect.com/journal/geomatica

Heatwave vulnerability of large metropolitans in Bangladesh: An evaluation

Mohammed Sarfaraz Gani Adnan [a,*], Irfat Kabir [b], Md Alamgir Hossain [c], Salit Chakma [d], Syeda Nazifa Tasneem [e], Champa Rani Saha [f], Quazi K. Hassan [g], Ashraf Dewan [h]

[a] Civil and Environmental Engineering (CEE), Brunel University London, Uxbridge UB8 3PH, United Kingdom
[b] Department of Urban and Regional Planning, Chittagong University of Engineering and Technology (CUET), Chittagong 4349, Bangladesh
[c] Economic Relations Division, Government of the People's Republic of Bangladesh, Dhaka, Bangladesh
[d] Department of Disaster Management and Resilience, Bangladesh University of Professionals, Dhaka 1216, Bangladesh
[e] Department of Geosciences, Auburn University, Haley Center, 2046, Auburn, AL 36849, United States
[f] Center for Environmental and Geographic Information Services (CEGIS), F-14/E, Administrative Area, Dhaka 1207, Bangladesh
[g] Department of Geomatics Engineering, University of Calgary, 2500 University Drive NW, Calgary Alberta T2N 1N4, Canada
[h] Spatial Sciences Discipline, School of Earth and Planetary Sciences, Curtin University, Perth 6102, Australia

ARTICLE INFO

Keywords:
Heatwave vulnerability
Exposure
Sensitivity
Adaptive capacity
Principal component analysis
Bangladesh

ABSTRACT

Heatwaves pose a significant risk to human society, and assessing vulnerability at the local scale is challenging due to the multifaceted nature of contributing factors. This study focuses on evaluating the heatwave vulnerability of five major cities in Bangladesh: Chittagong, Dhaka, Khulna, Rajshahi, and Sylhet. Heatwave vulnerability index (HVI) was estimated, integrating exposure, sensitivity, and adaptive capacity components. Time-series data from the Moderate Resolution Imaging Spectroradiometer (MODIS) for land surface temperature (LST) spanning 2000–2019 served as the primary dataset. The HVI calculation employed a principal component analysis method. The spatial distribution of the resulting HVI across five metropolitan areas were evaluated by estimating spatial autocorrelation and identifying clusters and hot spots in vulnerable areas. The findings revealed that urban centers characterized by extensive built-up areas exhibited higher exposure to urban heat compared to their surroundings. Dhaka, the capital, recorded the highest mean annual LST, while Sylhet registered the lowest. Rajshahi and Sylhet stood out for having the largest percentage of heat-exposed and sensitive areas, respectively. Sylhet also had the highest percentage of heat-vulnerable areas, reaching 63 %, whereas Dhaka had the highest number of vulnerable individuals, totaling 12.5 million. The findings also suggested that augmenting urban green and blue infrastructures holds potential for mitigating the adverse impacts of heatwaves. The methodology and outcomes of this study provide a valuable foundation for devising heatwave adaptation strategies not only in Bangladesh but also in other regions facing similar challenges.

1. Introduction

Heatwaves pose a severe threat to human well-being, with the urban heat island (UHI) exacerbating heat stress impacts [96]. The UHI phenomenon, characterized by higher air and surface temperatures in cities compared to surrounding areas, is attributed to factors such as dense urbanization, population growth, waste heat generation, and insufficient green spaces [46,54]. The escalating risks of morbidity and mortality due to heat stress are associated with extreme heat events, a trend expected to intensify with global climate change [54,66]. The Intergovernmental Panel on Climate Change (IPCC) warns of likely surpassing the 1.5 ℃ global warming threshold in the near future (2021–2040), especially under high greenhouse gas emission (SSP5–8.5) [38]. Dosio et al. [25] projected that a 1.5 ℃ global temperature increase could expose around 700 million people to extreme heatwave events (e.g., 1-in-20-year events). Furthermore, urban temperature rises contribute to a considerable spike in buildings energy consumption, with a 1 ℃ increase necessitating an extra 5 % energy usage for cooling [46].

Bangladesh is highly sensitive to a range of environmental stressors, including heatwaves [63]. During heatwave days, defined as the 95th percentiles of both day- and nighttime temperatures, the country is

* Corresponding author.
E-mail address: sarfaraz.adnan@brunel.ac.uk (M.S.G. Adnan).

https://doi.org/10.1016/j.geomat.2024.100020
Received 3 June 2024; Received in revised form 11 August 2024; Accepted 13 August 2024
Available online 15 August 2024

likely to experience a 22 % higher mortality rate [63,80]. The potential increase in heatwave frequency and intensity in the future is anticipated due to climate change, unplanned urbanization, and rapid industrial development [63,71]. According to Im et al. [36], the wet-bulb temperature, which represents the threshold of human survivability, is projected to exceed 35 ℃ by the end of the 21st century in various South Asian countries, including Bangladesh, under the RCP8.5 climate change scenario. Additionally, the number of nighttime heatwaves is expected to rise [85,86].

Various strategies, such as evaporative cooling, altering surface albedo, the use of shading, increasing greenery, and promoting urban green infrastructure (UGI), have proven effective in mitigating urban temperature rises [14,66,77]. The implementation of UGI, a network of planned green spaces, exhibits potential for reducing temperatures during hot and dry periods [66]. However, the effectiveness of these measures varies depending on spatial and temporal factors. For instance, shading is most effective during the day, providing comfort in street canyons, while high albedo measures and evaporative cooling are less effective [77]. The characteristics of vegetation cover, including architectural form, tree canopy density, patch size, edge, and connectivity, also influence urban heat [14,66].

Understanding spatiotemporal patterns of heatwave vulnerability is crucial for implementing effective mitigation strategies [65,91]. However, assessing vulnerability is challenging due to the influence of diverse location-specific factors, including meteorological, physical, socioeconomic, and environmental elements [8,9,97]. Typically, heatwave vulnerability encompasses three interrelated factors: exposure, sensitivity, and adaptive capacity [12,37,52]. Exposure gauges the threat level posed by heatwaves to people, infrastructure, and the environment, involving both environmental (e.g., temperature, humidity, wind) and anthropogenic (e.g., population, occupational health hazards) factors [52]. Sensitivity, or susceptibility, measures an individual's ability to withstand heatwave impacts and depends on socioeconomic (e.g., income, education, acclimatization), demographic, physiological (e.g., age, gender), geographic (e.g., distance to healthcare center), and health-related (e.g., body composition, pre-existing medical conditions) factors [5,8,9,52]. Adaptive capacity, the final component, reflects the ability of individuals, communities, or cities to adapt to heatwave effects and is associated with various mitigation (e.g., green infrastructure, tree canopy, water-sensitive urban design) and adaptation strategies (e.g., heat warning systems, individual heat adaptation measures) [37,52,71].

Globally, several studies have estimated heatwave vulnerability over the past few decades [9,12,13,16,91]. In Bangladesh, most of the heat-related studies have focused on the hazard component of vulnerability [4,21,24,63,64,71]. For instance, Nissan et al. [63] and Nissan et al. [64] correspondingly defined heatwaves and evaluated various climatic models to characterize these extreme heat events. [24] and [21] examined surface urban heat island intensity (SUHII) in five major cities, analyzing patterns, drivers, and diurnal and seasonal trends. In relation to the adaptive capacity component of vulnerability, Tawsif et al. [83] discussed household-level adaptation strategies to heatwaves in a medium-sized city, Rajshahi, in Bangladesh. Regarding heatwave vulnerability, specific investigations have focused on Chittagong and Dhaka, conducted by Raja [71] and Abrar et al. [4], respectively, using cross-sectional (i.e., data collected at one point or period) land surface temperature (LST) data.

However, the dynamic nature of urban warming and its impact on natural and anthropogenic environments over time and space, as evidenced in Bangladesh [21,24], introduces uncertainties when predicting heatwave vulnerability using cross-sectional analyses. To address the gap created by the lack of heatwave vulnerability studies incorporating longitudinal temperature data, this study aims to explore the factors governing in the spatial patterns of heatwave vulnerability across major metropolitan areas in Bangladesh, leveraging satellite-based time-series infrared temperature data.

2. Materials and methods

2.1. Study area

This study focused on five major cities in Bangladesh: Chittagong, Dhaka, Khulna, Rajshahi, and Sylhet (Fig. 1). These urban centers experience heightened urban heat stress due to substantial population growth, rapid urbanization, and a notable prevalence of impervious surfaces, particularly during the summer months [24]. The spatial expansion rates of these cities underscore the urbanization challenges, with Dhaka growing at an annual rate of 11.5 % [57], Rajshahi at 5.0 % [28], and Chittagong at 3.75 %. Abdullah [2]. The cumulative population across these cities is approximately 45.45 million, with Dhaka alone housing around 23 million residents [2]. Situated in a subtropical climate zone, these cities experience four distinct seasons: pre-monsoon (March–May), monsoon (June–September), post-monsoon (October–November), and winter (December–February) [24]. It is noteworthy that each of these cities is equipped with a single weather station capturing 3-hourly temperature data, limiting the revelation of spatial heat vulnerability patterns. Therefore, this study utilized quality-controlled time-series LST data to evaluate heatwave vulnerability, considering the strong correlation between satellite-based surface temperature data and air temperature [62].

2.2. Heat-related data

For this study, multi-year LST data was obtained from the Moderate Resolution Imaging Spectroradiometer (MODIS) — specifically, the MOD11A2 LST product (v006) — at a spatial resolution of 1 km spatial resolution, acquired by the Terra satellites. The data was acquired from the Terra satellites using a generalized split-window approach that involved extracting information from MODIS bands 31 and 32 [87]. Daily observations, captured at 10.30 am and 10.30 pm, spanning the years 2000 to 2019, were converted into annual composites. To ensure data accuracy, preprocessing steps were employed to correct cloud contamination. Only clear sky pixels exhibiting an LST error of ≤ 2 K were retained across all cities. The percentage of retained pixels varied across seasons and cities, with the post-monsoon period retaining the highest percentage. Further details on the distribution of retained pixels, following the removal of cloud-affected pixels, can be found in Dewan et al. [21]. A comprehensive methodology for MODIS data processing is available in Dewan et al. [24] and Dewan et al. [21].

2.3. Estimating heatwave vulnerability index (HVI)

Heatwave vulnerability index (HVI) was determined in this study using exposure (E), sensitivity (S), and adaptive capacity (A) variables (Eq. 1). Fig. 2 provides an overview of the methodology employed in this study.

$$HVI = E + S - A \tag{1}$$

All three components of the HVI underwent normalization by employing the min-max normalization technique (Eq. 2), which involved transforming their values into a standardized 0–1 scale. This approach was utilized to mitigate spatial bias arising from variations in unit measurements across HVI indicators. Subsequently, the resulting HVI underwent an additional normalization using the same procedure.

$$x' = \frac{x - \min(x)}{\max(x) - \min(x)} \tag{2}$$

where x' is the normalized value and x is the original value of an indicator.

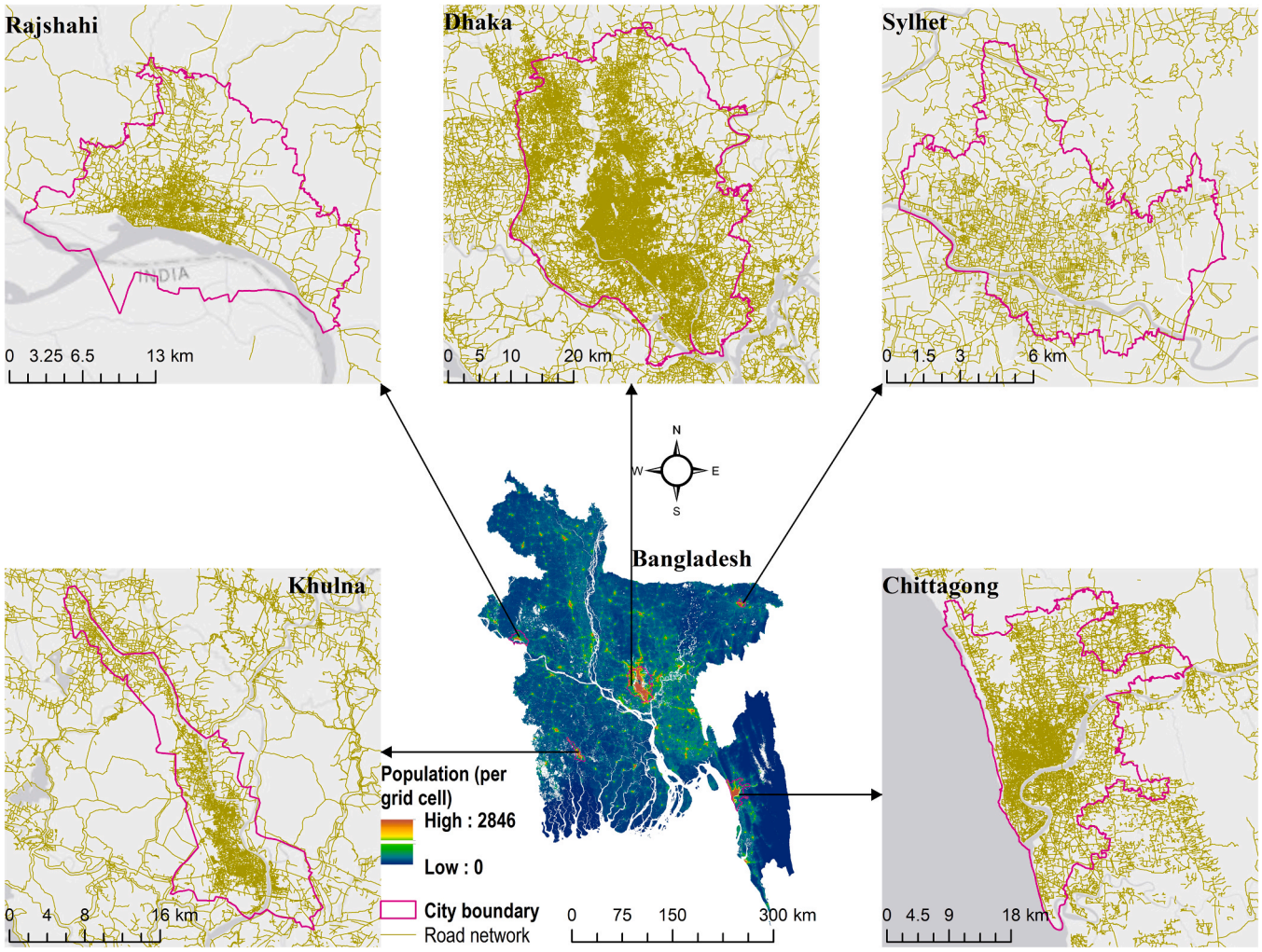

Fig. 1. Locations of five cities in Bangladesh.

2.4. *Selecting indicators for heatwave vulnerability*

In this research, a total of 23 variables were identified following a thorough examination of the extant literature. Indicators were categorized according to three broad components of HVI: exposure, sensitivity, and adaptive capacity. A detailed description of the selected indicators including their sources is given in Table 1.

2.4.1. *Exposure*

The exposure parameters encompassed various elements such as LST, population density, white-sky albedo (WSA), aerosol optical depth (AOD), nighttime lights (NTL), biophysical composition index (BCI), urban index (UI), and various physical and climatic factors such as elevation, relative humidity, and sunshine. The assessment of heat exposure in a specific zone relied on the extent and geographical distribution of temperature increases during heat-related events. Given the evolving impact of climate change and UHI phenomenon on heat exposure over time and space, it was essential to consider topographic features, land cover, and environmental factors in the analysis [30].

While air temperatures from meteorological stations are the conventional measure of heat exposure, in-situ measurements often fail to capture the spatial distribution of heat due to an insufficient number and sparse placement of weather stations [12]. Consequently, recent studies have increasingly used LST as an indicator of heat exposure because of its close correlation with air temperature [11,12,95]. Elevated LST is associated with higher rates of various heat-related diseases, including cardiovascular disease, diarrhea, and respiratory disease [37].

In this study, daily MOD11A2 LST products were used to estimate the annual average LST over the period 2000–2019 (see Section 2.2). MODIS LST offers a high spatial resolution of 1 km, which is particularly useful for capturing temperature variations across urban areas, thereby overcoming the limitations posed by the uneven distribution of weather stations. In contrast, other global data sources, such as the fifth-generation European Centre for Medium-Range Weather Forecasts (ECMWF) atmospheric reanalysis (ERA5) air temperature data, have a spatial resolution of 25 km [35], which is less effective in capturing localized heatwave effects within urban areas.

Seasonal LST values were estimated for the pre-monsoon (MAM), monsoon (JJAS), post-monsoon (ON), and winter (DJF) seasons. The LST values were then categorized into five temperature regions using Jenks' Natural Break classification system for each season: very low (<27.5 °C), low (27.6 °C to 28.3 °C), moderate (28.4 °C to 29.2 °C), high (29.3 °C to 30.4 °C), and very high (>30.5 °C).

NTL data was utilized to assess the impact of human activities, while the BCI was selected for its efficacy in distinguishing impermeable surfaces from other types of urban land cover [49]. Additional indicators of heat exposure included daily AOD, gridded population density, daily short-wave black and white sky albedo (WSA) and UI. Increased built-up areas can exacerbate heatwaves by retaining solar heat for longer periods than adjacent areas, leading to elevated regional temperatures. Moreover, regions with higher population densities are likely to experience significant anthropogenic heat emissions [60,73]. In addition to

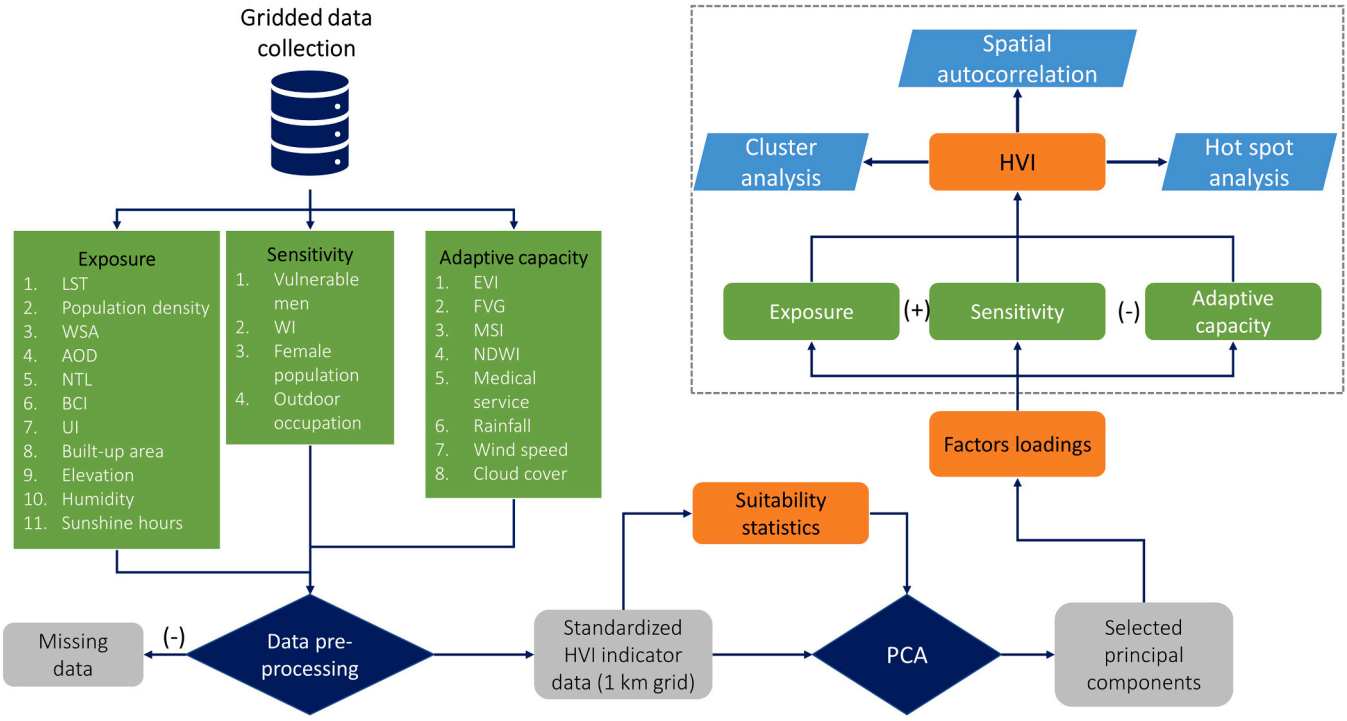

Fig. 2. Methodology flow diagram of this study.

built-up areas, UI was employed in this study for its ability to effectively differentiate between hard surfaces and bare land [59].

Relative humidity was also considered, as Mora et al. [58] established a link between surface air temperature, relative humidity, and 82 % of mortality during heatwaves. Data on various meteorological indicators, such as relative humidity and sunshine hours, were obtained as vector data from different meteorological stations. To convert these data into grids, the Inverse Distance Weighted (IDW) interpolation technique was applied. This method was chosen because, unlike temperature data, indicators like humidity and sunshine hours were not available at the high spatial resolution provided by MODIS. Thus, interpolation was necessary to create a continuous surface over the study area.

2.4.2. *Sensitivity*

Sensitivity signifies the inherent characteristic of a system that is prone to increased exposure. Four indicators related to sensitivity parameters were selected, including poverty (measured by wealth index), vulnerable men either aged < 9 years or over 65 years, total female population, and occupation (in the industrial or agricultural sectors). Older adults face increased vulnerability to heatwave due to factors such as age, diminished mobility, and underlying health conditions, including cardiovascular disorders [8,52]. Additionally, children under the age of nine and females are sensitive to heatwaves, as they are more susceptible to various vector-borne diseases. Furthermore, extreme heat events are correlated with various socioeconomic conditions. Individuals below the poverty line (with purchasing power parities (PPPs) <US$1.90/day) are at a higher risk of heatwaves due to a lack of facilities and adequate information on heatwave risks [56,68,70]. Occupations involving high levels of physical activity, such as agriculture and industrial work, contribute to heat vulnerability [18]. Similar to exposure, the resulting sensitivity map was categorized into five natural break classes.

2.4.3. *Adaptive capacity*

The indicators selected for assessing adaptive capacity in this study were particularly relevant for analyzing economic conditions and the overall well-being of the population [12,33]. Numerous factors can affect individuals' ability to adapt to environmental challenges, including demographics, health, access to resources, support, and information (such as heat protection measures), as well as mobility. Wolf and McGregor [91] emphasized that an individual's sensitivity to heat is shaped by these factors. Therefore, the selection of indicators should align closely with the need to analyze economic conditions and population well-being, as adaptive capacity is fundamentally linked to human responses to external changes [12,33].

In this study, eight variables were identified as potentially mitigating the adverse effects of heatwaves. These variables included the enhanced vegetation index (EVI), moisture stress index (MSI), fraction of green vegetation (FVG), normalized difference water index (NDWI), access to medical services, and various meteorological factors such as rainfall, wind speed, and cloud cover (Table 1). Gridded layers of EVI, MSI, FVG, and NDWI, derived from MODIS data, were obtained from Dewan et al. [21].

Both EVI and FVG were used as vegetation-related indicators because they provide unique and complementary information. EVI optimizes the vegetation signal by correcting for atmospheric conditions and canopy background noise, making it particularly effective in areas with dense vegetation [55]. Conversely, FVG directly measures the proportion of green vegetation, offering a straightforward and interpretable metric for vegetative cover extent [29]. Using both EVI and FVG allows for a more nuanced and robust assessment of vegetation's role in adaptive capacity, especially under varying environmental conditions.

To determine access to medical centers, the Euclidean distance from each hospital location was computed. The distance to hospitals and general practitioners within the study area serves as an indicator of the average level of healthcare available in that region. A higher value suggests that an area is less vulnerable to heatwaves due to adequate infrastructure, frequent medical services, and the presence of general practitioners during such periods [12]. Although some hospital locations provided information on hospital capacity (i.e., the number of hospital beds), this indicator was excluded from the analysis due to a significant number of missing data. The hospital location data were superimposed on a 1 km grid to calculate the capacity of hospitals within corresponding grids. The resulting adaptive capacity layer was also

Table 1
Indicators of heatwave vulnerability.

Indicators		Association with heatwave vulnerability	Resolution / Format	Data source
Latent	Observed			
Exposure	Land surface temperature (LST)	LST is closely linked to air temperature, serving as an indicator of heatwaves [95].	Daily MODIS MOD11A2 LST product (v006) at 1 km spatial resolution	Wan [88]
	Population density	Rapid population growth contributes to urban expansion, poverty, congestion, changes in climatic conditions, and a decline in waterbodies, consequently elevating vulnerability to heatwaves [17, 90].	Number of people per grid cell at 100 m resolution	WorldPop [92]
	Albedo (WSA)	Albedo refers to the Earth's reflectivity. Surfaces with low albedo have the potential to amplify surface thermal stress and increase mortality rates [43,76,80].	Daily MODIS MCD43A3 product at 500 m spatial resolution	Schaaf [78]
	Aerosol optical depth (AOD)	AOD serves as an indicator of pollutant concentration in the environment, and its levels are positively correlated with heat stress [93].	Daily MODIS MCD19A2 product at 1 km spatial resolution	Lyapustin [51]
	Nighttime lights (NTL)	NTLs serve as a manifestation of anthropogenic activity on the Earth's surface. NTL data aids in extracting urban areas by monitoring city lights at night (Dewan et al., 2021; Li et al., 2019). The NTL data utilized in this study includes information from the Defense Meteorological Satellite Program – Operational Linescan system (DMSP-OLS) and the Visible Infrared Imaging Radiometer Suite (VIIRS).	Gridded data (Yearly)	Dewan [21]
	Biophysical composition index (BCI)	BCI defines the imperviousness of a surface, exhibiting a positive correlation with urban heat stress.	Estimated from MODIS data at 1 km spatial resolution	Dewan [21]
	Urban Index (UI)	UI indicates the presence of hard surfaces. It is a crucial determinant, as the development of structural expansions and congested urban areas all contribute to heightened vulnerability [21,31].	Estimated from MODIS data at 1 km spatial resolution	Dewan [21]
	Built-up areas	Percentage of land cover classified as built-up area. Heat exposure is linked to the extent of built-up areas, with a high proportion of this land cover type indicating elevated exposure levels.	Extracted from ESRI land cover data	Karra [44]
	Elevation	Topographical factors such as surface elevation shows a slight association with heat stress and play a significant role among different geographical regions [58].	Gridded data at 30 m resolution	Jaxa [39]
	Relative humidity	Relative humidity is an important indicator in defining heat waves as it is directly related to human body heat exchange [15]. Monthly average humidity data from 1988 −2012, across different weather stations, are collected from Bangladesh Agricultural Research Council (BARC).	Vector data	http://www.barc.gov.bd/
	Sunshine hours	Daylight hour is an indicator of heat exposure. Monthly average daylight hour	Vector data	http://www.barc.gov.bd/

(*continued on next page*)

Table 1 (*continued*)

Indicators		Association with heatwave vulnerability	Resolution / Format	Data source
Latent	Observed			
		data from 1988 −2012, across different weather stations, are collected from Bangladesh Agricultural Research Council (BARC).		
Sensitivity	Vulnerable men (Age <=9 or >= 65 years)	Vulnerable men include male populations aged either below 9 years or above 65 years. Older adults over 65 are more susceptible to the effects of urban heat due to ongoing health issues. Children under the age of nine are also more vulnerable to heatwaves than adults due to their lower sweating levels and mass index [37,91].	Number of people per grid cell at 100 m resolution	WorldPop [92]
	Wealth index	Poverty is linked to poor housing, inadequate nutrition, and restrictive socioeconomic conditions, rendering people more sensitive to heatwaves [5, 37].	Gridded demographic health index (DHS) wealth index data at 1 km resolution	Steele [82]
	Female population	Women respond differently to heatwaves compared to men due to their larger body fat percentages and less physical strength [71, 94].	Number of people per grid cell at 100 m resolution	WorldPop [92]
	Occupied in industrial or agricultural sectors	Individuals engaged in outdoor work, such as agricultural and industrial labor, are more susceptible to heatwaves [5, 91].	Number of people employed in industrial agricultural sector	De Bono [19]
Adaptive capacity	Enhanced Vegetation Index (EVI)	EVI is an optimized vegetation index that is designed to enhance the vegetation signal by improving sensitivity in high biomass regions and reducing atmospheric and canopy background noise. EVI is particularly useful in regions with high vegetation density. A high percentage of green cover and reduced vulnerability to heatwaves are indicators of a higher EVI score [37,71].	Estimated from MODIS data at 1 km spatial resolution	Dewan [21]
	Fraction of Green Vegetation (FVG)	FVG, representing the fraction of green vegetation, indicates the presence of vegetation canopies. A high FVG is associated with lower urban heat levels [72].	Estimated from MODIS data at 1 km spatial resolution	Dewan [21]
	Moisture stress index (MSI)	The MSI, reflecting soil and plant moisture levels, provides insights into the temperature conditions of urban areas [21, 73].	Estimated from MODIS data at 1k m spatial resolution	Dewan [21]
	Normalized Difference Water Index (NDWI)	NDWI was utilized for detecting waterbodies. A high NDWI value indicates the presence of more waterbodies, reducing susceptibility to heatwaves [37, 91].	Estimated from MODIS data at 1 km spatial resolution	Dewan [21]
	Distance to medical services	The accessibility of healthcare facilities is linked to heatwave vulnerability, as enhancing access to such facilities has the potential to reduce vulnerability during heatwave events. The determination of access to medical centers involves measuring the distance (in kilometers) from an area to the	Inostroza et al., [37,45]	Spatial data, UNISDR

(*continued on next page*)

Table 1 (*continued*)

Indicators		Association with heatwave vulnerability	Resolution / Format	Data source
Latent	Observed			
		nearest health facility [5,45].		
	Meteorological factors (Rainfall, windspeed, cloud cover)	Rainfall, wind speed, and cloud cover are crucial meteorological parameters for mitigating the potential impact of heat stress.	Gridded rainfall data at 1 km resolution. Station data of windspeed and cloud cover	Dewan [22]

categorized into five classes applying Jenks' Natural Break classification system. Climatic variables, including wind speed and cloud cover data, were obtained from various meteorological stations. The IDW interpolation technique was applied to convert these point data into continuous grids.

2.5. Statistical analyses

2.5.1. Data preprocessing

This study employed principal component analysis (PCA) to estimate HVI. Heat vulnerability-related studies often employ PC due to its ability to convert correlated variables into linearly uncorrelated principal components, hence, reducing the dimensionality of the data [16]. PCA is a multivariate exploratory technique designed to synthesize core aspects of a sample, encompassing measurements for various quantitative variables across multiple individuals [26,41]. Prior to conducting standard PCA, several steps of data processing were executed. This study was conducted at a spatial resolution of 1 km, aligning with the resolution of the MODIS LST datasets. Considering the diverse resolution and data types (i.e., vector and raster) of variables related to heatwave vulnerability, various approaches were employed to consolidate the dataset within the 1 km grid. Section 2.4 outlines the methods used to process layers of different HVI indicators. All datasets were standardized applying Eq. 2 prior to the PCA application.

The resulting database contained some missing values. To maintain consistency in the database, missing value imputation was performed. PCA and other standard multivariate algorithms use the eigendecomposition of a cross-product matrix. For PCA to construct an ordination of observations, a complete data matrix is required, consistent with other matrix algebra techniques [26,69]. Instead of ignoring or removing observations with incomplete values, this study utilized the 'missMDA' function in the R programming language [42] for imputing missing data. This function employs principal component methods on incomplete data with multiple imputation techniques, considering both individual similarity and the link between the variables. Multiple imputation techniques were utilized to address the issue of overestimating variance, resulting from the imputation of missing values [75]. The imputation process generated several sets of imputed data, illustrating the potential variation in the prediction of missing values.

2.5.2. Suitability of PCA

To assess the suitability of PCA, this study estimated Pearson's correlation coefficients to detect collinearity between different variables. All variables were included to determine the appropriateness of both independent factors and factor combinations. Significance tests at the 95 % and 99 % levels, along with Pearson's correlation coefficient (r), were conducted. Fig. S1 in the supplementary document shows Pearson's correlation coefficients among different indicators of HVI across five different cities. Since some of the indicators, particularly related to the sensitivity component, are correlated between each other, PCA was deemed to be suitable for this study.

2.5.3. Principal component analysis (PCA)

PCA was conducted individually for each of the five cities and three components of HVI (exposure, sensitivity, and adaptive capacity) separately. The Kaiser-Meyer-Olkin (KMO) measure and Bartlett's test of sphericity were computed to assess the applicability of individual factors and variable combinations. For Bartlett's test of sphericity, a p-value less than 0.1 was considered statistical significance. KMO values exceeding 0.50 (on a scale from 0 to 1) indicated sampling adequacy [67]. The study found KMO values for exposure parameters ≥ 0.50 in all five cities, and for sensitivity and adaptive capacity, KMO values ranged from 0.68 to 0.73 and 0.59 to 0.65, respectively. Bartlett's test of sphericity yielded significant p-values for all instances (Table 2).

Next, all factors were weighted using the variance-weighted technique [79]. A combined principal component (PC) score (z-score) was derived by integrating the variance explained by different factors [91]. To determine the number of components to retain, three approaches were followed: scree plots, Kaiser's criterion, and retaining PCs that combinedly explained at least 80 % of the variance. Factor loadings were estimated, and varimax rotation plots [1] were developed to explain all factors under each PC.

2.6. Analyzing spatial distribution patterns of HVI

The spatial distribution of HVI across five metropolitan areas were assessed by estimating spatial autocorrelation and identifying clusters and hot spots in vulnerable areas.

2.6.1. Estimating spatial autocorrelation

In this study, spatial autocorrelation of HVI was measured using Global Moran's I statistic [32]. This index helps determine whether the overall HVI is clustered, dispersed, or random. Moran's I values can be positive, negative, or zero. Positive values indicate a tendency toward clustering, negative values indicate dispersion, and zero suggests a random distribution with no autocorrelation. The significance of the index is evaluated using the associated z-score and p-value. To reject a null hypothesis of randomly distributed data, p-values should be less than 0.05 at a 95 % confidence interval, z-scores should be less than -1.96 or greater than $+1.96$. The Moran's I statistic can be calculated using the following equation:

$$I = \frac{n}{S_o} \frac{\sum_{i=1}^{n}\sum_{j=1}^{n} w_{i,j} z_i z_j}{\sum_{i=1}^{n} z_i^2} \tag{3}$$

where z_i is the deviation of an attribute for feature i from its mean $(x_i - \overline{X})$, w_{ij} is the spatial weight between feature i and j, n is equal to the total number of features, and S_o is the aggregate of all the spatial weights:

$$S_o = \sum_{i=1}^{n}\sum_{j=1}^{n} w_{i,j} \tag{4}$$

2.6.2. Identifying spatial clusters of HVI

While the Global Moran's I provides an understanding of overall

Table 2
Kaiser-Meyer-Olkin (KMO) measure and Bartlett's test of sphericity.

Cities	Exposure		Sensitivity		Adaptive capacity	
	KMO	Bartlett's p-value	KMO	Bartlett's p-value	KMO	Bartlett's p-value
Chittagong	0.73	2.2e−16	0.5	2.2e−16	0.65	2.2e−16
Dhaka	0.73	2.2e−16	0.67	2.2e−16	0.65	2.2e−16
Khulna	0.72	2.2e−16	0.5	2.2e−16	0.64	2.2e−16
Rajshahi	0.68	2.2e−16	0.61	2.2e−16	0.59	2.2e−16
Sylhet	0.68	2.2e−16	0.61	2.2e−16	0.59	2.2e−16

spatial distribution pattern of HVI, identifying spatial clusters requires estimating the Anselin local Moran's *I* index [6]. This index measures local spatial correlations to identify the type of spatial correlation between two variables [16]. The local Moran's *I* index was calculated utilizing the following equation:

$$I_i = \frac{x_i - \overline{X}}{S_i^2} \sum_{j=1,\ j\neq i}^{n} w_{i,j}\left(x_j - \overline{X}\right) \tag{5}$$

where x_i is an attribute for feature i, $\overline{X}$ is the mean of the corresponding attribute, $w_{i,j}$ is the spatial weight between feature i and j, n is the total number of features, and:

$$S_i^2 = \frac{\sum_{j=1,\ j\neq i}^{n}\left(x_j - \overline{X}\right)^2}{n-1} \tag{6}$$

The statistical significance of the estimated index was determined by *z*-score and *p*-value. Significant positive index values indicate clusters, while negative values indicate outliers. Anselin [7] classified local Moran's *I* index values into four categories: cluster of high values (HH), cluster of low values (LL), an outlier with a high value surrounded by low values (HL), and an outlier with a low value surrounded by high values (LH) [16].

2.6.3. Identifying hot spots of HVI

This study further identified hot spots of HVI by calculating the Getis-Ord Gi* statistic [32]. The Gi* statistic identifies hot spots by evaluating a cell in the context of its neighboring cells. A cell is considered a statistically significant hot spot if it has a high value and is surrounded by other cells with high values. Conversely, a cold spot occurs when a cell has a very low value and is surrounded by other cells with low values. The Gi* statistic can be calculated using the following equation:

$$G_i^* = \frac{\sum_{j=1,}^{n} w_{i,j}x_j - \overline{X}\sum_{j=1}^{n} w_{i,j}}{S\sqrt{\frac{\left[n\sum_{j=1}^{n} w_{i,j}^2 - \left(\sum_{j=1}^{n} w_{i,j}\right)^2\right]}{n-1}}} \tag{7}$$

where x_j is the attribute value for cell j, $w_{i,j}$ is the spatial weight between cell i and j, n is equal to the total number of cells and:

$$\overline{X} = \frac{\sum_{j=1}^{n} x_j}{n} \tag{8}$$

$$S = \sqrt{\frac{\sum_{j=1}^{n} x_j^2}{n} - (\overline{X})^2} \tag{9}$$

The output of the Gi*statistic is a *z*-score for each cell, which represents the statistical significance of clustering within a specified distance. The *z*-score represents the statistical significance of clustering for a specified distance. At a 95 % confidence level, a *z*-score less than −1.96 or greater than 1.96 indicates statistically significant hot spot.

2.7. Validating proxy temperature data

Previous studies employed various methods to validate HVI, including the analysis of above-average mortality or ambulance callout rates during heatwave days, as well as examining changes in health outcomes associated with increased heat vulnerability [53,91]. The predominant focus in these approaches was on mortality rates and ambulance callouts during heatwave events [10]. However, such data are not available in the context of Bangladesh. Consequently, this study conducted a validation test on LST data derived from MODIS, which serves as the primary indicator of heat exposure. For this purpose, bivariate regression models were developed for five case study cities, using monthly MODIS LST data from 2000 to 2019 as the dependent variable and observed near-surface air temperature at the same temporal resolution as the independent variable. These models were instrumental in assessing the accuracy with which LST explained near-surface air temperature. To represent the observed air temperature, this study utilized ERA5 air temperature data at a height of 2 m above the surface of land, sea, or inland waters [35]. Recent studies also found consistencies between ERA5 and MODIS LST [89]. The resulting coefficient of determination (R^2) values elucidated the degree of agreement between MODIS LST and ERA5 2 m air temperature.

3. Results

3.1. Heatwave exposure

Various degrees of heat exposure were evident across different times and locations. Across all five cities, the urban cores exhibited higher temperatures than the surrounding outskirts (supplementary Fig. S3). Dhaka city registered the highest annual mean LST at 32.13 °C, while Sylhet recorded the lowest at 25.6 °C. City centers in Dhaka, Chittagong, and Khulna showed a higher LST compared to those in Sylhet and Rajshahi. However, suburbs in all cities were consistently characterized by low thermal intensity. The thermal intensity extended along the road networks, with central areas of Dhaka, Chittagong, and Rajshahi labeled as having an above-moderate thermal intensity. In Dhaka, the northeastern part, predominantly occupied by wetlands, exhibited the lowest annual mean LST.

Fig. 3 depicts the historical trends of the mean annual surface temperature over 20 years (2000–2019). Generally, the mean temperature in pre-monsoon seasons exceeded that of other seasons, ranging between 28 °C and 34.5 °C. Pre-monsoon temperature trends varied significantly among the five cities, with Rajshahi consistently having a higher pre-monsoon surface temperature. Notably, 2010 recorded relatively lower temperatures in Rajshahi, while 2008 and 2019 saw the highest temperatures.

During the monsoon season, mean LST in different cities exhibited no consistent trend, with Sylhet showing higher mean LST compared to the other four cities. Chittagong, on the other hand, had lower temperatures. In the post-monsoon season, a minor yearly temperature variation was observed across the five cities, with Dhaka having the highest post-monsoon LST. In winter, all cities experienced lower temperatures than in other seasons. Although differences in mean temperatures among cities were not prominent, Dhaka and Chittagong saw a marginal increase in LST from 2005 to 2019, with an increase in yearly temperature by 0.8 °C and 0.2 °C, respectively. Khulna and Rajshahi recorded lower mean LST in the winter season than the other three cities.

The PCA results reveal the diverse contributions of different factors to various principal components. In regard to heat exposure category, PCA extracted three components in all cities, except for Rajshahi, where four components were identified, collectively explaining at least 80 % of the total variance. The first component (PC1) explains the highest variance. For instance, PC1 in Chittagong, Dhaka, and Khulna contributed to over 40 % of the total variance. In Rajshahi and Sylhet, the variance contributions of the first PC were 34 % and 24.7 %, respectively (see Supplementary Fig. S2).

Varimax rotations shown in Fig. 4 visually illustrate the results of applying PCA with varimax rotation to a set of variables. In this plot, arrows represent variables, and their directions and lengths provide insights into their contributions to the rotated principal components (PC1 and PC2). Circular correlation patterns in the plot indicate that the rotated components are uncorrelated or orthogonal, simplifying the interpretation of underlying patterns. The position of each arrow along the PC1 and PC2 axes indicates the variable's strength and direction in relation to these components. The plot elucidates which variables have similar or opposing effects on the principal components.

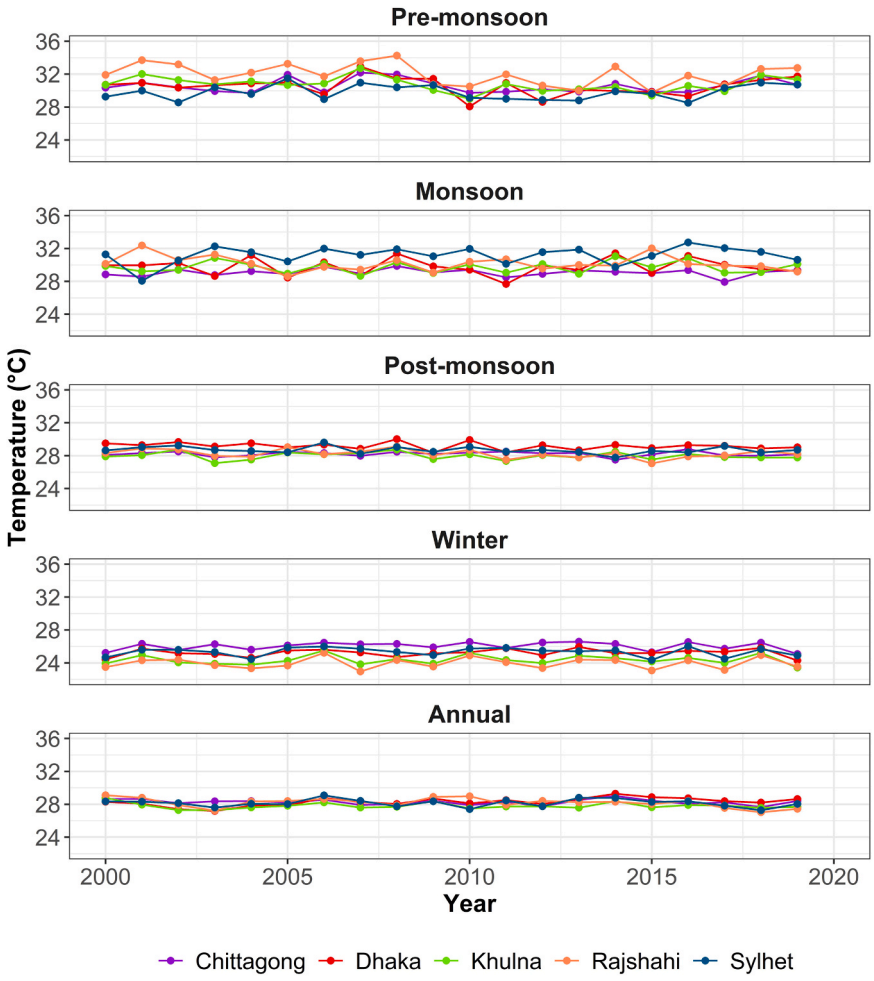

Fig. 3. Historical surface temperature trends in five cities, 2000–2019.

Fig. 4 reveals several clusters among the 11 indicators of heat exposure. For instance, in Chittagong, three clusters were observed: cluster 1 (AOD, BCI), cluster 2 (UI, NTL, LST, built-up area, population density), and cluster 3 (sunshine hours, humidity, WSA, elevation). Generally, factors within cluster 2 such as UI, NTL, LST, and built-up areas, exerted the highest level of influence on the selected PCs in all cities. This observation was further supported by the estimated factor loadings presented in Table 3.

The spatial pattern and distribution of heat-exposed areas are shown in Fig. 5 and Fig. 9, respectively. The proportion of heatwave-exposed zones, ranging from moderate to very high degrees, varied from 45.3 % in Chittagong to 70.2 % in Rajshahi. In Dhaka, an estimated 59.4 % of the total area was considered heat exposed.

3.2. Heatwave sensitive zones

The PCA results for sensitivity component showed that the first principal component (PC1) accounted for more than 60 % of the total variances for all cities, except Khulna (supplementary Fig. S2). Factors such as vulnerable age groups of men and women exhibited positive association with the PC1 and PC2 in all cities except for Khulna and Sylhet. In Sylhet, poverty was positively correlated with PC1 and PC2 (see Fig. 4 and Table 3). Fig. 6 shows the spatial distribution of heat-sensitive zones in five cities. The proportion of heat-sensitive zones of moderate to very high severity ranged from 13.7 % in Chittagong to 29.8 % in Sylhet of the total area, respectively. In Dhaka, 15.5 % of the total area was estimated to be heat-sensitive (Fig. 9).

3.3. Heatwave adaptive capacity

After five iterations, variable rotations in the assessment of heatwave adaptive capacity resulted in three PCs with eigenvalues greater than 1. These PCs played a crucial role in highlighting the likely differences between indicators of capacity and mitigation measures for heatwave vulnerability. n Dhaka, Chittagong, Rajshahi, and Sylhet, three successive PCs exhibited variance proportions of 80 %, 79 %, 77 %, and 78 %, respectively. Khulna, on the other hand, showed that the combination of two components accounts for 68 % of the total variance (refer to Fig. S2 in supplementary document).

The influence and nature of the association between various indicators of adaptive capacity and the PCs vary across different cities. For example, in Chittagong, hospital distance and rainfall exhibited a positive association with both PC1 and PC2. In Khulna, such a positive association was observed with FVG and EVI (see Fig. 4 and Table 3).

Fig. 7 illustrates the spatial distribution of areas adaptive to heatwave vulnerability. Generally, the core city areas showed lower heat adaptive capacity. The percentage of the total city area adaptive to heatwave ranged from 48.2 % in Sylhet to 87.1 % in Rajshahi. In Chittagong, Dhaka, and Khulna, the proportion of areas adaptive to heatwave was estimated to be 85.3 %, 79.3 %, and 78.8 %, respectively (Fig. 9).

3.4. Heatwave vulnerability in major cities

HVI maps were generated to portray the spatial distribution of heatwave vulnerability in the five major cities of Bangladesh. The

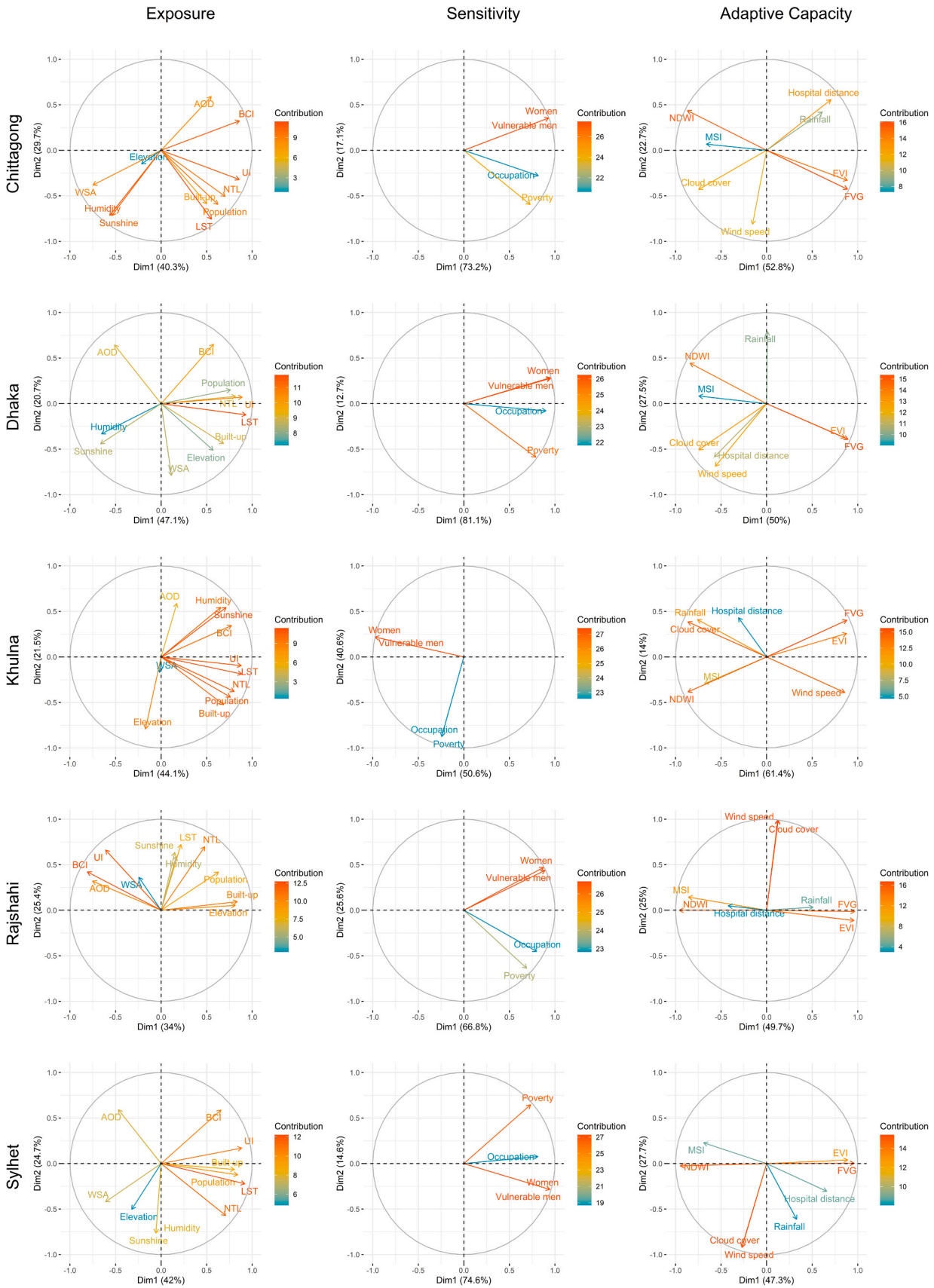

Fig. 4. Varimax rotation showing clusters of heat exposure, sensitivity, and adaptive capacity parameters in five cities. Here, 'Dim 1' and 'Dim 2' indicate principal component 1 (PC1) and principal component 2 (PC2), respectively.

Table 3
Variables loading for exposure, sensitivity, and adaptive capacity.

Indicator		Chittagong			Dhaka			Khulna			Rajshahi				Sylhet		
Latent	Observed	PC1	PC2	PC3	PC1	PC2	PC3	PC1	PC2	PC3	PC1	PC2	PC3	PC4	PC1	PC2	PC3
Exposure	AOD	−0.26	−0.33	0.09	−0.22	−0.43	−0.09	−0.08	0.38	0.33	−0.39	0.19	−0.15	0.18	−0.22	0.36	−0.40
	BCI	−0.41	−0.18	−0.21	0.25	−0.43	0.32	−0.35	0.22	−0.23	−0.42	0.25	−0.12	0.27	0.31	0.36	−0.28
	LST	−0.26	0.42	0.07	0.41	0.08	0.03	−0.40	−0.12	0.25	0.11	0.43	−0.21	−0.31	0.43	−0.13	0.01
	NTL	−0.33	0.28	0.15	0.36	−0.05	0.20	−0.36	−0.25	−0.11	0.25	0.42	−0.13	0.26	0.33	−0.35	0.10
	UI	−0.41	0.18	−0.02	0.39	−0.05	0.15	−0.40	−0.06	0.19	−0.31	0.40	−0.26	0.01	0.41	0.10	−0.20
	WSA	0.36	0.21	0.13	0.05	0.52	−0.40	0.01	−0.11	0.79	−0.13	0.22	−0.06	−0.81	−0.28	−0.26	−0.10
	Population	−0.30	0.33	0.15	0.34	−0.10	0.14	−0.35	−0.29	−0.06	0.33	0.25	−0.34	0.21	0.39	−0.08	0.17
	Built-up area	−0.24	0.32	−0.12	0.30	0.29	0.02	−0.31	−0.34	0.05	0.43	0.06	−0.20	0.09	0.38	−0.04	−0.01
	Elevation	0.10	0.08	0.88	0.25	0.34	0.16	0.08	−0.51	−0.25	0.42	0.03	−0.09	−0.14	−0.15	−0.31	0.49
	Humidity	0.27	0.39	−0.23	−0.29	0.22	0.58	−0.30	0.35	−0.17	0.09	0.35	0.59	0.06	−0.03	−0.46	−0.47
	Sunshine	0.26	0.40	−0.24	−0.29	0.29	0.53	−0.32	0.35	−0.11	0.08	0.38	0.56	0.05	−0.03	−0.46	−0.47
Sensitivity	Poverty	0.43	N/A	N/A	0.44	N/A	N/A	−0.17	−0.69	N/A	0.42	−0.63	N/A	N/A	0.42	N/A	N/A
	Vulnerable Men	0.55	N/A	N/A	0.53	N/A	N/A	−0.69	0.17	N/A	0.55	0.43	N/A	N/A	0.55	N/A	N/A
	Women	0.55	N/A	N/A	0.53	N/A	N/A	−0.69	0.17	N/A	0.53	0.46	N/A	N/A	0.55	N/A	N/A
	Occupation	0.48	N/A	N/A	0.50	N/A	N/A	−0.17	−0.69	N/A	0.49	−0.45	N/A	N/A	0.47	N/A	N/A
Capacity	EVI	0.43	−0.25	−0.06	0.43	−0.25	0.06	0.40	0.18	N/A	0.48	−0.08	0.02	N/A	0.46	0.03	−0.02
	FVG	0.43	−0.32	−0.01	0.45	−0.27	0.06	0.40	0.32	N/A	0.49	−0.01	0.04	N/A	0.49	0.01	0.04
	MSI	−0.32	0.05	0.38	−0.37	0.06	0.04	−0.31	−0.23	N/A	−0.43	0.10	0.04	N/A	−0.36	0.15	−0.07
	NDWI	−0.42	0.32	−0.03	−0.42	0.30	−0.07	−0.39	−0.30	N/A	−0.48	0.00	−0.04	N/A	−0.49	−0.02	−0.04
	Hospital distance	0.34	0.41	0.27	−0.29	−0.39	−0.05	−0.14	0.34	N/A	−0.21	0.04	0.00	N/A	0.34	−0.20	−0.31
	Rainfall	0.30	0.31	0.42	0.00	0.53	0.07	−0.34	0.36	N/A	0.26	0.03	−0.10	N/A	0.17	−0.41	−0.17
	Wind Speed	−0.08	−0.60	0.33	−0.28	−0.46	0.01	0.39	−0.33	N/A	0.06	0.70	0.05	N/A	−0.13	−0.62	0.04
	Cloud cover	−0.36	−0.32	0.11	−0.37	−0.34	0.01	−0.39	0.32	N/A	0.06	0.70	0.05	N/A	−0.14	−0.62	0.04

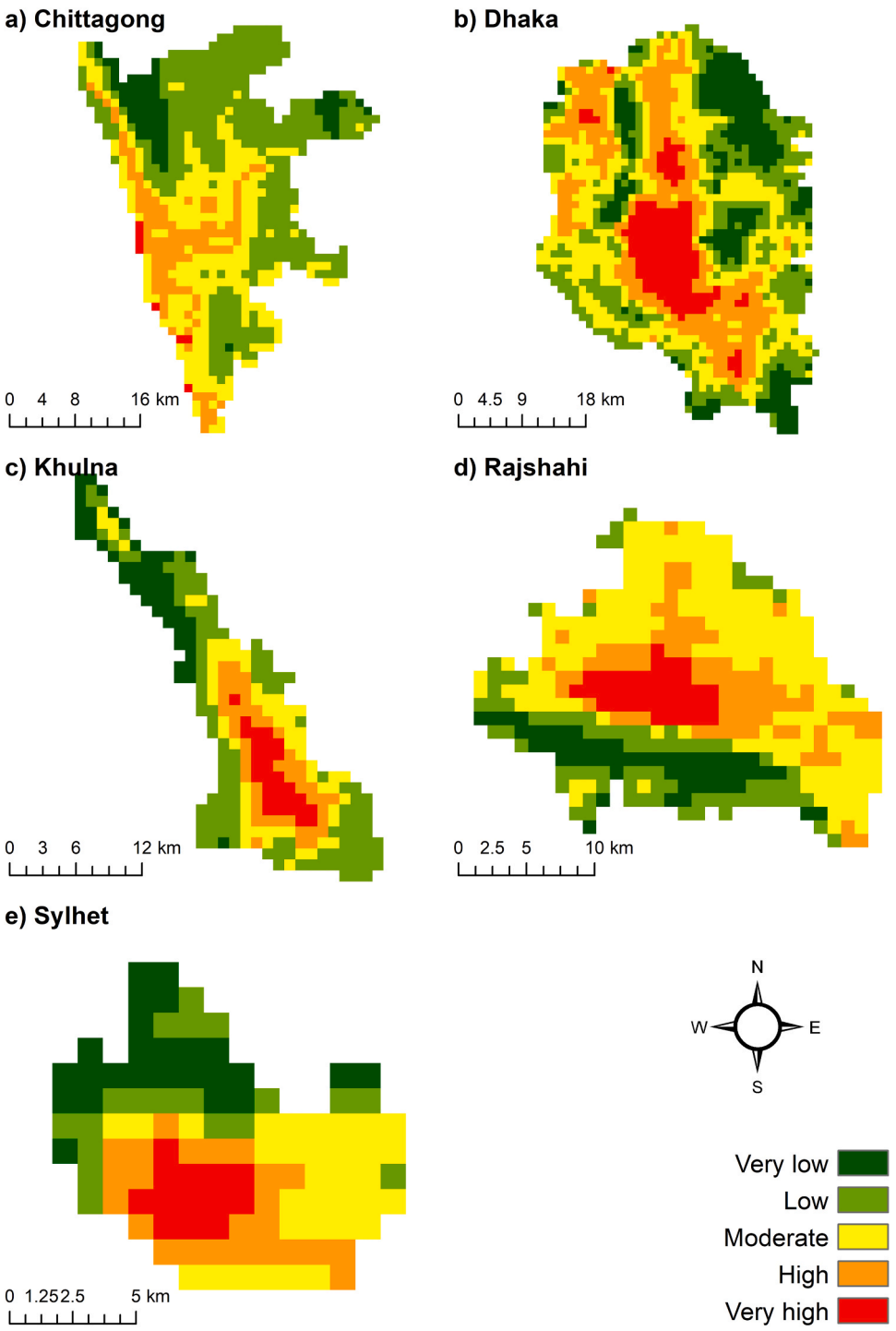

Fig. 5. Spatial distribution of heat exposure in five cities.

resulting layers of exposure, sensitivity, and adaptive capacity were incorporated into Eq. 1 to generate heatwave vulnerability maps. Each city was subdivided into five categories based on heatwave vulnerability levels: very low, low, moderate, high, and very high, using Jenks' Natural Break classification system (Fig. 8). Areas exhibiting normalized HVI closer to zero were designated as low-vulnerability zones, while those with normalized HVI values closer to 1 were identified as highly vulnerable areas. Similar to regions exposed to heat, areas in proximity to the city center in various cities demonstrated higher vulnerability compared to the outskirts (Fig. 8).

In most cities, a significant proportion of areas were identified as vulnerable to heatwaves. Sylhet emerged as the region with the highest percentage of vulnerable areas, with 63 % of the total area susceptible to heatwaves of moderate to extreme severity. Chittagong, Dhaka, Khulna, and Rajshahi cities had 39 %, 31 %, 50 %, and 25 % of vulnerable areas, respectively. Regarding the vulnerable population, Dhaka had the largest number of heatwave-vulnerable individuals, totaling 12.5 million (equivalent to 77.7 % of the total population). It was followed by Chittagong (2.9 million or 72.8 %), Khulna (0.7 million or 69.2 %), Sylhet (0.5 million or 83.1 %), and Rajshahi (0.4 million or 44.9 %).

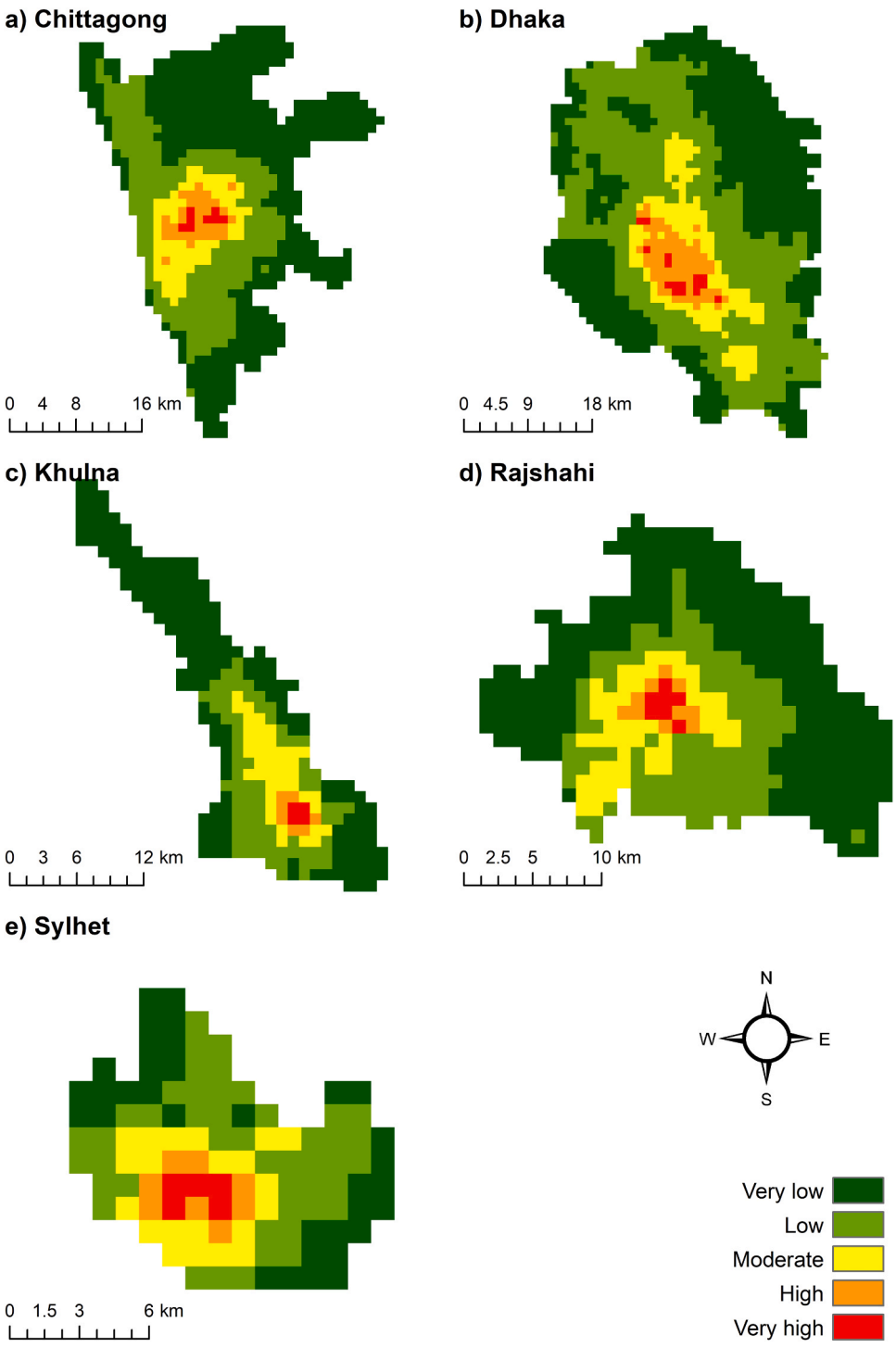

Fig. 6. Heatwave sensitive zones in the five cities of Bangladesh.

3.5. Spatial distribution of HVI

After estimating the HVI, this study aimed to analyze the spatial distribution patterns of heatwave vulnerabilities by assessing spatial autocorrelation, clusters and outliers, and hot spots. The Global Moran's *I* results for all five cities indicated positive values with significant *z*-scores and *p*-values (Table 4), suggesting a non-random, clustered patterns of HVI across these metropolitan areas.

While the Global Moran's *I* coefficient provided an overview of HVI distribution, the Anselin Local Moran's *I* coefficient was used to identify specific clusters and outliers within each city (Fig. 10). In all five metropolitan areas, high-high clusters (indicated in red) were predominantly located in the core urban zones. These areas exhibited high HVI values surrounded by other highly vulnerable areas, underscoring their significant susceptibility to heatwaves. Conversely, the outskirts of the cities were more likely to have low-low clusters, where low HVI values were surrounded by less vulnerable areas, indicating regions with lower heatwave vulnerability.

The identification of these clusters is critical for understanding localized vulnerability. High-high clusters in densely populated and economically significant central city areas suggest a concentration of factors that exacerbate vulnerability, such as high population density,

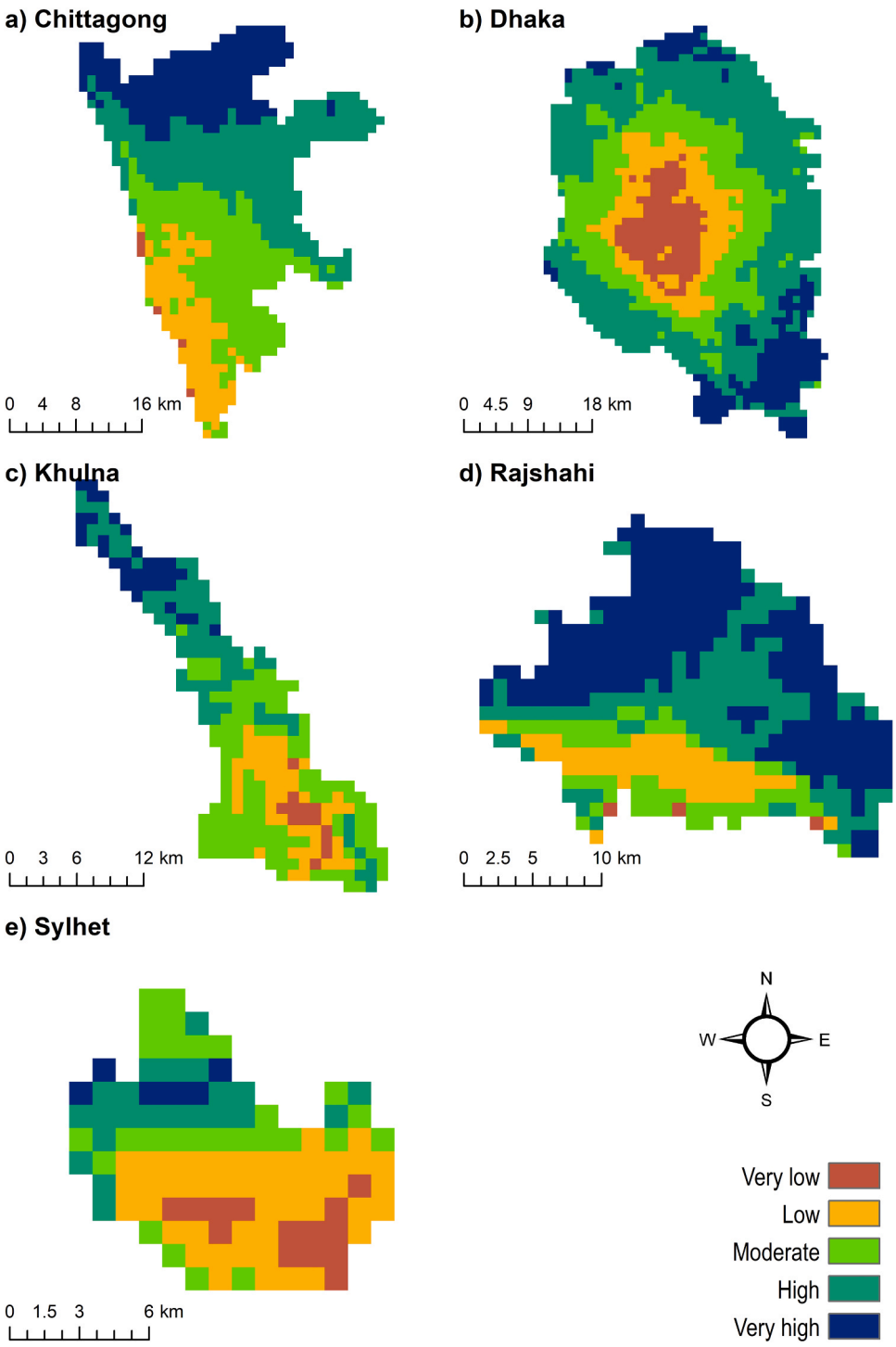

Fig. 7. Spatial patterns of adaptive capacity to heatwave impacts.

reduced vegetation, and increased impervious surfaces.

Additionally, the hot spot analysis was conducted using the Getis-Ord Gi* index provided further granularity by classifying clusters into hot and cold spots with varying confidence intervals (Fig. 11). Central city areas, particularly business districts, emerged as significant hot spots at the 99 % confidence interval, indicating areas with intense heatwave vulnerability. As the confidence interval decreased, the extent of the hot spot areas expanded, encompassing a broader portion of the urban core. This trend underscores the widespread nature of heatwave vulnerability in these urban centers.

4. Discussion

Investigating heatwave vulnerability in rapidly expanding urban areas in Bangladesh is critical due to the increasing risks associated with extreme temperatures and prolonged periods of the anomalous heat [40, 73]. This study aimed to estimate Heat Vulnerability Index (HVI) using a principal component analysis (PCA) method, derived from multiple variables related to heat exposure, sensitivity, and adaptive capacity, in the five rapidly growing metropolitans of Bangladesh: Chittagong, Dhaka, Khulna, Rajshahi, and Sylhet.

The PCA results revealed varying contributions of different factors to

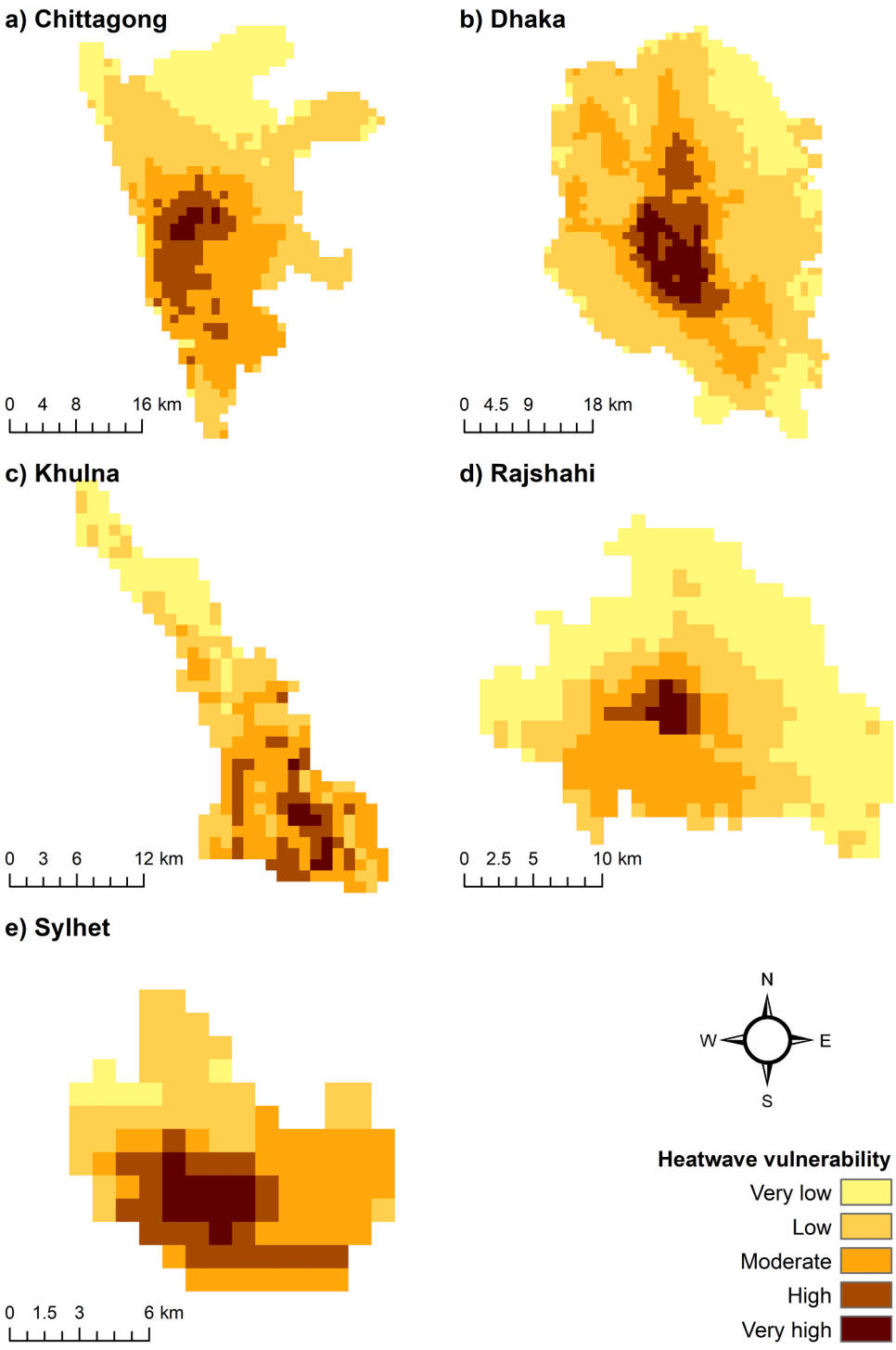

Fig. 8. Spatial distribution of heatwave vulnerability in five cities.

various principal components, changing significantly between cities. This variation is likely due to differences in urban morphology, socio-economic factors, and local climatic conditions [37]. The findings of this study underscore that all five cities are highly exposed to heatwaves, with over 45 % of their total areas facing increased vulnerability. Rajshahi exhibited the highest degree of heat exposure. In terms of Land Surface Temperature (LST), Rajshahi experienced higher mean pre-monsoon surface temperatures than other cities between 2000 and 2019. However, Dhaka had the highest annual mean surface temperature of 32.13 °C, while Sylhet recorded the lowest at 25.6 °C. High LST and urbanization factors such as a substantial Urban Index (UI), Nighttime Light (NTL), and built-up areas were significantly associated with this heat exposure. Many recent studies have found a positive association between built-up areas and LST [27,37,71,74]. The study suggests that increasing urbanization amplifies surface temperatures due to impervious surfaces enhancing evaporation and a lack of infiltration, and high-density structures trapping and emitting heat throughout day and night. Building density and road infrastructure also influence LST [34,60], a phenomenon evident in Dhaka and Rajshahi due to rapid urbanization over the past decades [21,24].

This study further identified heat sensitive zones using different indicators, including age, gender, economic status, and occupation.

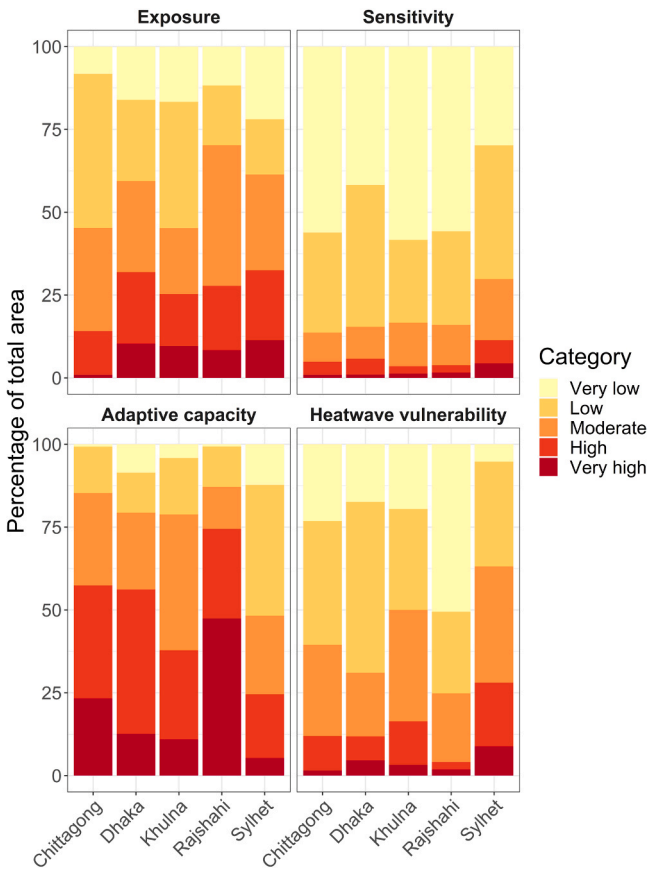

Fig. 9. Comparison of exposure, sensitivity, adaptive capacity, and heatwave vulnerability in five cities.

Table 4
Results of spatial autocorrelation analysis.

Cities	Moran's *I*	Variance	*z*-score	*p*-value
Chittagong	0.94	0.0006	37.17	0.0000
Dhaka	0.93	0.0003	53.49	0.0000
Khulna	0.83	0.002	19.99	0.0000
Rajshahi	0.94	0.001	27.55	0.0000
Sylhet	0.87	0.005	12.65	0.0000

Vulnerability was notably high in areas with large number of women and men aged either < 9 years or > 65 years, aligning with the findings from existing studies [37,71,73,91]. Senior citizens are particularly at risk due to social isolation and thermal stress [50,61,84]. Intense heatwaves exacerbate existing health conditions and contribute to various health issues such as hypertension, coronary heart disease, nephrolithiasis, pulmonary illnesses, heat exhaustion, and heat stroke [20,48]. Children, especially in urban areas, are highly vulnerable due to climate change and urban heat islands [12].

Moreover, factors such as poverty (indicated by the wealth index) and specific occupations (e.g., agricultural, and industrial labor) demonstrated positive correlations with HVI. Low-income residents in warmer regions lacking green infrastructure were more susceptible, while high-income residential areas with low-density development and ample green space were less affected [37,40]. Sylhet stood out among the five cities, with the highest proportion (29.8 %) of heat-sensitive areas, driven by a significant number of vulnerable individuals and a large agricultural workforce.

The study identified several adaptive capacity indicators that can potentially mitigate the impacts of heatwaves. Increased vegetation, soil moisture, and water bodies can aid in mitigating the adverse effects of heatwaves [5,71]. Notably, Chittagong (85.3 %) and Rajshahi (87.1 %) had the highest proportions of areas adaptive to heatwave impacts. Sylhet exhibited the highest vegetation cover, while Dhaka had the lowest. Rajshahi and Chittagong also surpassed Dhaka in terms of vegetation cover, with Rajshahi benefiting from its proximity to the Ganges River and Chittagong being a coastal city with high waterbody and wetland proportions.

The lack of vegetation cover is a significant factor intensifying urban warming in Bangladesh, as identified in various studies [21,23,24,71]. Therefore, protecting existing green spaces and strategically planning the location of new vegetation patches in areas prone to urban heating should be a priority for urban planners. Although increasing soil moisture or creating new water bodies might be challenging for policymakers, there are actionable strategies that can be implemented to enhance urban resilience to heatwaves. These include the restoration and preservation of wetlands, especially in areas like Dhaka, where wetland degradation has been linked to rising land surface temperatures [3,4]. Dhaka, in particular, has experienced a significant decline in wetlands, which were initially identified as crucial water retention zones in the Dhaka Metropolitan Development Plan (1995–2015). The degradation of these wetlands has contributed to increased heat exposure, underscoring the urgent need for effective wetland restoration plans [3]. Additionally, urban planning should focus on integrating green and blue infrastructure, such as parks, green roofs, and artificial ponds, to enhance soil moisture retention and cooling effects in urban areas. These interventions not only help in mitigating the effects of heatwaves but also contribute to broader goals of urban sustainability and climate resilience.

The spatial distribution analyses (e.g., spatial autocorrelation, cluster, and hot spot analyses) of HVI indicated that vulnerability varied across different cities, revealing two predominant patterns. First, vulnerability tended to radiate from the core city to the suburbs in all cities, with central areas characterized by high vulnerability. For instance, within Dhaka and Chittagong, city corporation areas were identified as vulnerable hot spots, consistent with previous studies [4,71]. The centralization of administrative and commercial activities contributes to higher LST in core city areas, marked by increased built-up areas, reduced vegetation, and less water cover [4,21,24,71]. Second, a spatial vulnerability pattern emerged from the littoral land to the inland areas, influenced by a decrease in moisture stress or sea surface temperature impact. This finding complies with the existing studies [34]. Coastal regions, such as Chittagong and Khulna, exhibited higher heatwave duration but lower intensity, while inland areas experienced the opposite trend. Cities near riverbanks, like Dhaka and Rajshahi, showed increasing heat intensity from the banks to inland areas.

Moreover, the identification of high-high clusters and hot spots in central urban zones underscores the concentrated nature of heatwave vulnerability in these regions. Policymakers should prioritize these hot spots for interventions that increase vegetation, enhance cooling infrastructure, and restore wetlands. The strong spatial autocorrelation indicated by high Moran's *I* values suggests that these interventions could have widespread benefits, potentially reducing heatwave vulnerability across larger areas.

5. Limitations and future research directions

While this study provides valuable insights into high-resolution gridded heatwave vulnerability data, certain limitations and avenues for future research should be considered. One notable limitation is the absence of data on anthropogenic heat production (e.g., waste heat generation), urban morphology (e.g., sky view factor), and climatic conditions (e.g., wind direction) due to data unavailability. The accuracy of the results is also contingent on the precision of input data, particularly remote sensing data, where satellite-based LST measurements could potentially overestimate surface temperatures [21]. To

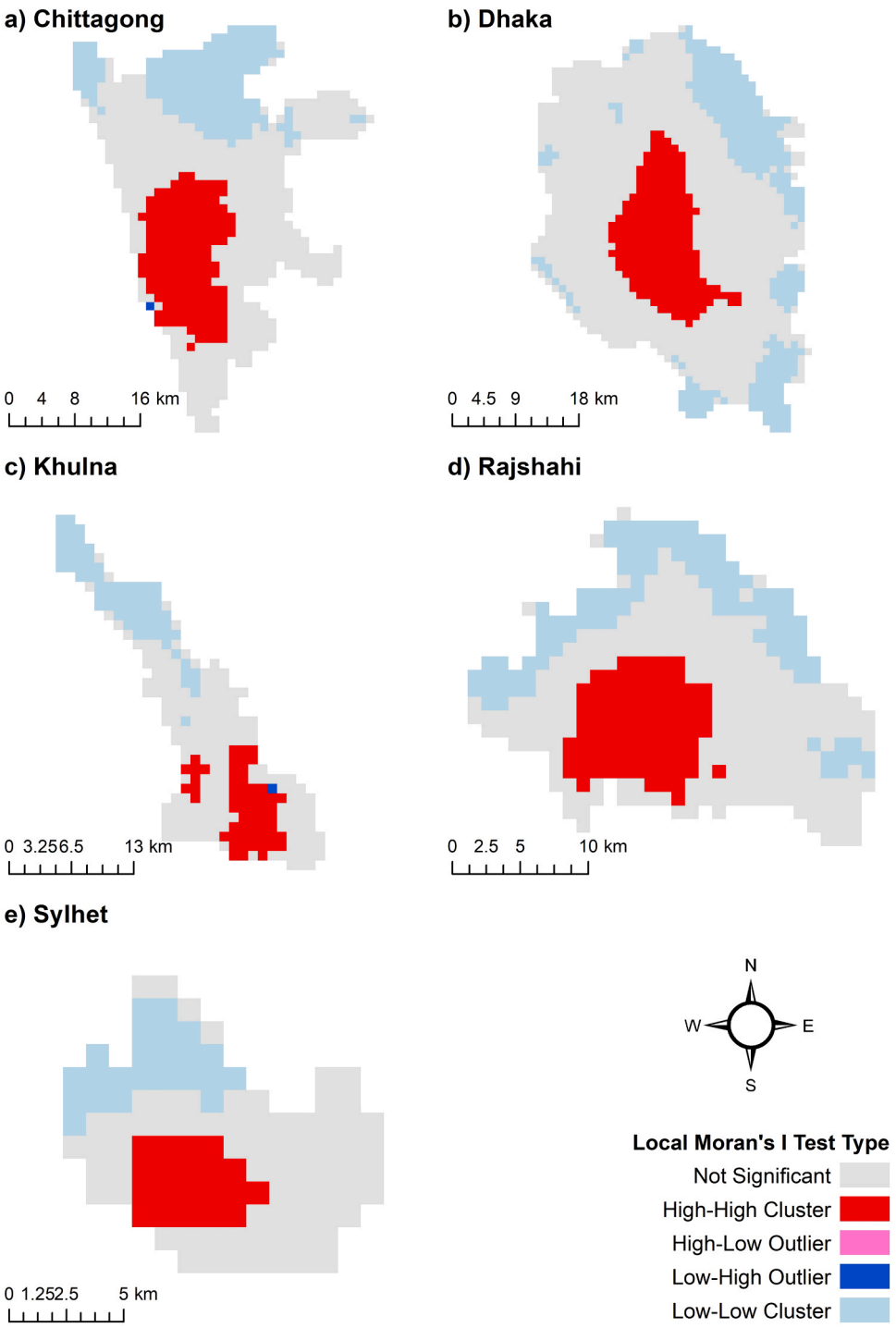

Fig. 10. Spatial patterns (Anselin Local Moran's I) of HVI.

address this issue, incorporating station-based observed data could provide more accurate assessments and help in refining the model.

Understanding the temporal variability of heatwave vulnerability is also crucial, given the dynamic nature of climate change, which affects the frequency, intensity, and duration of heatwaves over time [81]. Although this study utilized time series data on heat exposure, it did not assess the temporal variability in heatwave vulnerability due to the lack of time-series data on the different vulnerability indicators listed in Table 1. Future research should aim to address these gaps to enhance the understanding of heatwave vulnerability over time.

Uncertainties in the study arise from the differing resolutions and structures of input datasets. Gridded datasets, such as elevation and land cover, having finer resolutions at 30 m and population at 100 m, were extracted at 1 km grids, potentially leading to a loss of important variations within the 1 km zone. The use of IDW interpolation for station-based datasets, available in vector format at specific locations, may introduce noise in the grids. Future research should prioritize improving input datasets to enhance the reliability of such studies.

The use of LST as a proxy variable for defining heatwaves may introduce uncertainties. However, in this study, monthly LST was validated against monthly ERA5 2 m temperature data across five cities, demonstrating a reasonable degree of agreement (Fig. 12). The

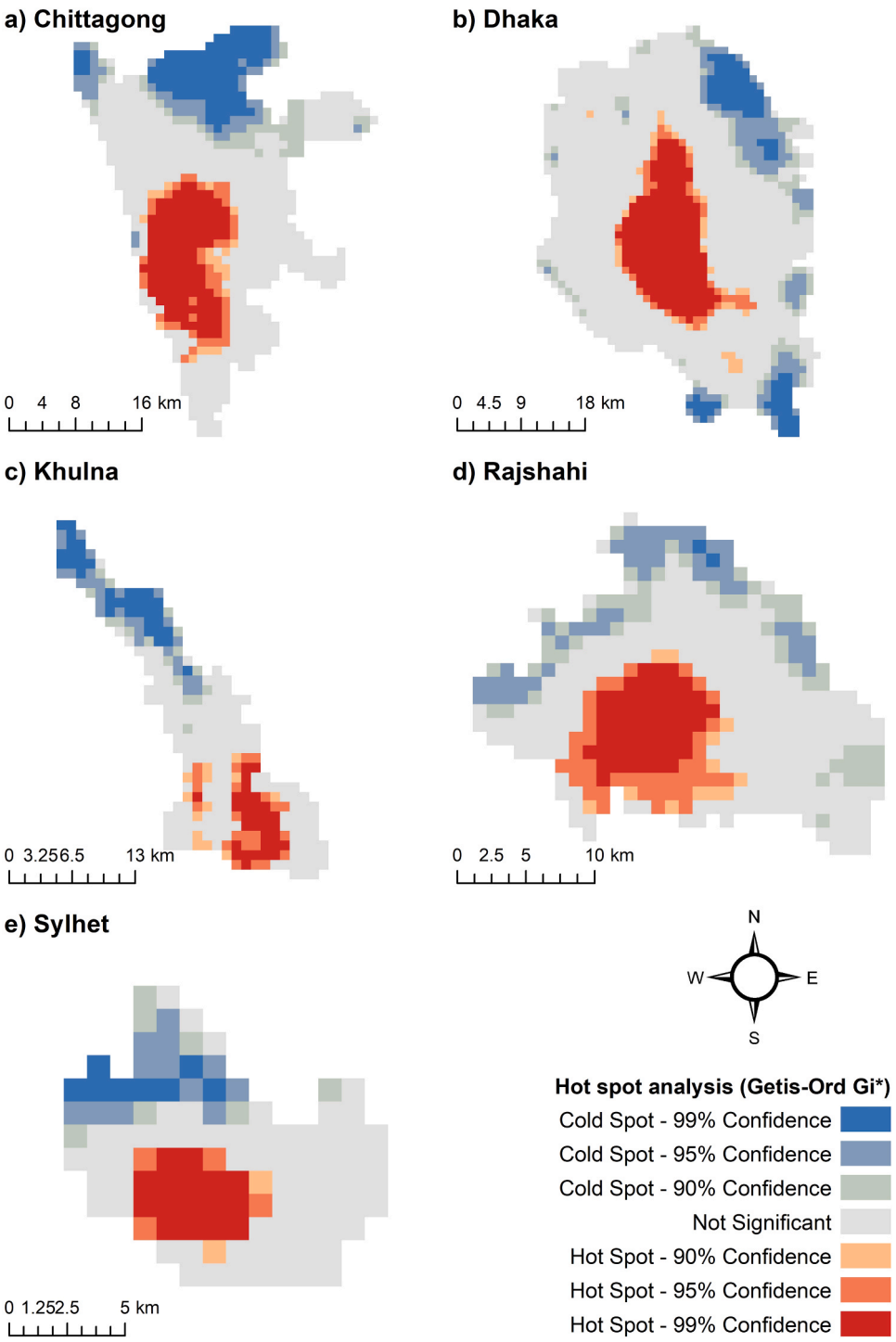

Fig. 11. Hot spots (Getis-Ord Gi*) of HVI.

coefficient of determination (R^2) values, representing the strength of the relationship between the two variables, exceeded 0.5 in all cities, with Khulna exhibiting the highest R^2 value at 0.81, followed by Rajshahi (0.76), Sylhet (0.67), Dhaka (0.66), and Chittagong (0.57). Future research could explore alternative global datasets, such as those from the Copernicus Climate Data Store, with higher temporal resolutions (e.g., hourly, daily) for defining heatwave events using air temperature data. Additionally, climate model outputs could be utilized to estimate potential heatwave vulnerability in the future.

Finally, it is important to consider the potential impact of spatial autocorrelation, as indicated by the high Moran's *I* values, on the results of the PCA used to derive the HVI. High spatial autocorrelation can influence the PCA results by artificially inflating the importance of certain variables, leading to the potential overemphasis of spatially clustered factors in the vulnerability assessment. Therefore, while these spatial analyses are valuable for identifying vulnerable areas, it is essential to interpret the results in the context of the spatial dependencies inherent in the data. Addressing these issues in future research could refine the accuracy of vulnerability assessments and enhance the applicability of findings to other urban contexts.

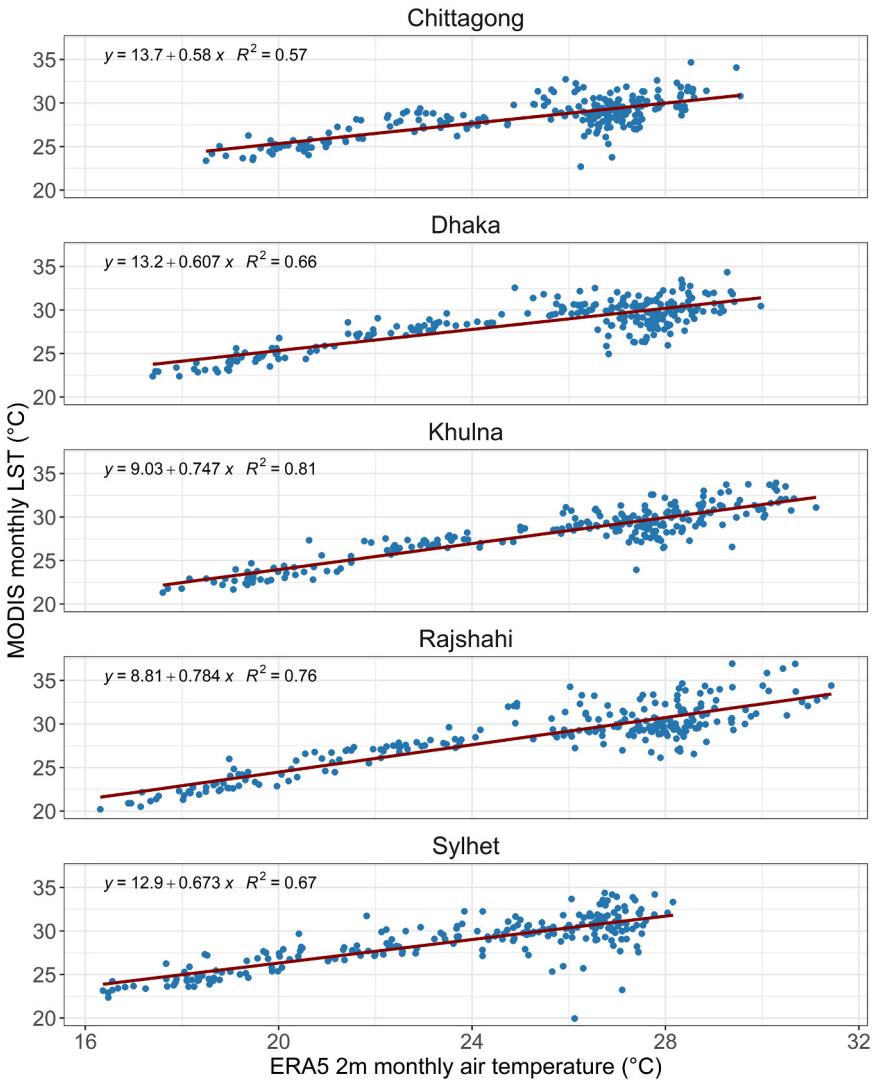

Fig. 12. Degree of agreement between ERA5 2 m monthly air temperature and MODIS monthly LST in different cities.

6. Conclusion

This study aimed to assess the spatial patterns of heatwave vulnerability in five major cities of Bangladesh: Chittagong, Dhaka, Khulna, Rajshahi, and Sylhet. Employing principal component analysis (PCA), this study estimated heatwave vulnerability through the Heat Vulnerability Index (HVI), considering heat exposure, sensitivity, and adaptive capacity. The findings revealed a substantial proportion of vulnerable areas in each city, with Dhaka having the highest number of heatwave-vulnerable individuals. Key factors associated with heat exposure included high surface temperature, rapid urbanization, and increased proportion of built-up areas.

The study identified populations highly sensitive to heatwaves, including the female population and young and elderly male. Economic status and occupation type were also linked to heat sensitivity, highlighting socio-economic disparities in vulnerability. Notably, green surfaces, wetlands, and high soil moisture were identified as having the highest adaptive capacity to heatwaves, underlining the importance of natural infrastructure in mitigating heat impacts.

Despite its limitations, this study contributes to understanding intra- and inter-urban variability in heatwave vulnerability in climate-sensitive regions. By incorporating more detailed local data and performing a comprehensive analysis, more targeted recommendations can be developed for urban green infrastructure to mitigate heatwave impacts. This study underscores that increasing vegetation cover, enhancing urban parks, and implementing green roofs and walls are potential strategies to reduce heatwave vulnerability in urban areas. Such insights are crucial for developing mitigation plans to alleviate the adverse impacts of urban warming-induced heatwaves [47]. The findings can inform the development of adaptation strategies for heatwaves not only in the five major cities studied but also serve as a methodology applicable to other locations for mapping heatwave vulnerability.

In conclusion, proactive urban planning and strategic investments in green infrastructure are essential for enhancing the resilience of cities to heatwaves. The methodology and results of this study can guide policymakers and urban planners in prioritizing areas and populations most at risk, thereby fostering more sustainable and resilient urban environments. Moving forward, integrating climate models and higher-resolution datasets could further refine vulnerability assessments and improve the efficacy of urban heatwave mitigation strategies.

Funding and acknowledgement

This work is funded by the Directorate of Research and Extension (DRE) of Chittagong University of Engineering and Technology (CUET) [grant number - CUET/DRE/2021–22/URP/011]. We are pleased to express our gratitude to the Department of Urban and Regional Planning of Chittagong University of Engineering and Technology for providing

logistic support to carry out this study.

CRediT authorship contribution statement

Mohammed Sarfaraz Gani Adnan: Writing – review & editing, Writing – original draft, Visualization, Validation, Project administration, Methodology, Funding acquisition, Formal analysis, Conceptualization. **Irfat Kabir:** Software, Methodology, Formal analysis. **Md Alamgir Hossain:** Writing – review & editing, Investigation, Data curation. **Salit Chakma:** Software, Resources, Investigation, Data curation. **Syeda Nazifa Tasneem:** Software, Resources, Investigation, Data curation. **Champa Rani Saha:** Software, Resources, Investigation, Data curation. **Quazi K. Hassan:** Writing – review & editing, Validation, Resources, Investigation. **Ashraf Dewan:** Writing – review & editing, Validation, Supervision, Conceptualization.

Declaration of Competing Interest

The authors declare that they have no known competing financial interests or personal relationships that could have appeared to influence the work reported in this paper.

Data availability

Data will be made available on request.

Appendix A. Supporting information

Supplementary data associated with this article can be found in the online version at doi:10.1016/j.geomat.2024.100020.

References

[1] H. Abdi, L.J. Williams, Principal component analysis, Wiley Interdiscip. Rev.: Comput. Stat. 2 (4) (2010) 433–459.
[2] S. Abdullah, et al., Investigating the impact of land use/land cover change on present and future land surface temperature (LST) of Chittagong, Bangladesh Earth Syst. Environ 6 (1) (2022) 221–235.
[3] H.M. Abdullah, et al., Development at the cost of unsustainable degradation of wetlands: Unraveling the dynamics (historic and future) of wetlands in the megacity Dhaka. *World Development*, Sustainability 4 (2024) 100131.
[4] R. Abrar, et al., Assessing the spatial mapping of heat vulnerability under urban heat island (UHI) effect in the dhaka metropolitan area, Sustainability 14 (9) (2022) 4945.
[5] M.S.G. Adnan, et al., Vulnerability of Australia to heatwaves: A systematic review on influencing factors, impacts, and mitigation options, Environ. Res. 213 (2022) 113703.
[6] L. Anselin, Local indicators of spatial association—LISA, Geogr. Anal. 27 (2) (1995) 93–115.
[7] L. Anselin, Exploring spatial data with GeoDaTM: a workbook, Cent. Spat. Integr. Soc. Sci. 1963 (2005) 157.
[8] C. Aubrecht, D. Özceylan, Identification of heat risk patterns in the US National Capital Region by integrating heat stress and related vulnerability, Environ. Int. 56 (2013) 65–77.
[9] G. Azhar, et al., Heat wave vulnerability mapping for India, Int. J. Environ. Res. Public Health 14 (4) (2017) 357.
[10] J. Bao, X. Li, C. Yu, The construction and validation of the heat vulnerability index, a review, Int. J. Environ. Res. Public Health 12 (7) (2015) 7220–7234.
[11] S. Bhattacharjee, et al., Assessment of different methodologies for mapping urban heat vulnerability for Milan, Italy. ed, IOP Conf. Ser.: Earth Environ. Sci. (2019) 012162.
[12] A. Buzási, Comparative assessment of heatwave vulnerability factors for the districts of Budapest, Hungary, Urban Clim. 42 (2022) 101127.
[13] J. Chambers, Global and cross-country analysis of exposure of vulnerable populations to heatwaves from 1980 to 2018, Clim. Change 163 (1) (2020) 539–558.
[14] S. Chapman, et al., The impact of urbanization and climate change on urban temperatures: a systematic review, Landsc. Ecol. 32 (2017) 1921–1935.
[15] X. Chen, et al., Global heat wave hazard considering humidity effects during the 21st century, Int. J. Environ. Res. Public Health 16 (9) (2019) 1513.
[16] T.-L. Chen, H. Lin, Y.-H. Chiu, Heat vulnerability and extreme heat risk at the metropolitan scale: a case study of Taipei metropolitan area, Taiwan, Urban Clim. 41 (2022) 101054.
[17] A. Costello, et al., Managing the health effects of climate change: lancet and University College London Institute for Global Health Commission, lancet 373 (9676) (2009) 1693–1733.
[18] S.L. Cutter, B.J. Boruff, W.L. Shirley, Social vulnerability to environmental hazards, Soc. Sci. Q. 84 (2) (2003) 242–261.
[19] A. De Bono, B. Chatenoux. A Global Exposure Model for GAR 2015, the Global Assessment Report on Disaster Risk Reduction 2015, from United Nations Office for Disaster Risk Reduction (UNISDR), 2014.
[20] F. de Galiza Barbosa, et al., Genitourinary imaging. Clinical PET/MRI, Elsevier,, 2023, pp. 289–312.
[21] A. Dewan, et al., Surface urban heat island intensity in five major cities of Bangladesh: patterns, drivers and trends, Sustain. Cities Soc. (2021) 102926.
[22] A. Dewan, et al., Developing a high-resolution gridded rainfall product for Bangladesh during 1901–2018. *Scientific*, Data 9 (1) (2022) 471.
[23] A.M. Dewan, R.J. Corner, Spatiotemporal Analysis of Urban Growth, Sprawl and Structure, in: A. Dewan, R. Corner (Eds.), Dhaka Megacity, Springer Geography. Springer, Dordrecht, 2014, https://doi.org/10.1007/978-94-007-6735-5_6.
[24] A. Dewan, G. Kiselev, D. Botje, Diurnal and seasonal trends and associated determinants of surface urban heat islands in large Bangladesh cities, Appl. Geogr. 135 (2021) 102533.
[25] A. Dosio, et al., Extreme heat waves under 1.5C and 2C global warming, Environ. Res. Lett. 13 (5) (2018) 054006.
[26] S. Dray, J. Josse, Principal component analysis with missing values: a comparative survey of methods, Plant Ecol. 216 (2015) 657–667.
[27] K. Ezimand, A. Kakroodi, M. Kiavarz, The development of spectral indices for detecting built-up land areas and their relationship with land-surface temperature, Int. J. Remote Sens. 39 (23) (2018) 8428–8449.
[28] M.I. Faridatul, Spatiotemporal effects of land use and river morphological change on the microclimate of Rajshahi metropolitan area, J. Geogr. Inf. Syst. 9 (4) (2017) 466–481.
[29] F. Filipponi, et al., Global MODIS fraction of green vegetation cover for monitoring abrupt and gradual vegetation changes, Remote Sens. 10 (4) (2018) 653.
[30] H.-M. Füssel, Vulnerability: a generally applicable conceptual framework for climate change research, Glob. Environ. Change 17 (2) (2007) 155–167.
[31] K.M. Gabriel, W.R. Endlicher, Urban and rural mortality rates during heat waves in Berlin and Brandenburg, Germany, Environ. Pollut. 159 (8-9) (2011) 2044–2050.
[32] A. Getis, J.K. Ord, The analysis of spatial association by use of distance statistics, Geogr. Anal. 24 (3) (1992) 189–206.
[33] S. Hajat, M. O'Connor, T. Kosatsky, Health effects of hot weather: from awareness of risk factors to effective health protection, lancet 375 (9717) (2010) 856–863.
[34] B.-J. He, et al., An approach to examining performances of cool/hot sources in mitigating/enhancing land surface temperature under different temperature backgrounds based on landsat 8 image, Sustain. Cities Soc. 44 (2019) 416–427.
[35] Hersbach, H., *et al.* , 2023. ERA5 monthly averaged data on single levels from 1940 to present. *Copernicus Climate Change Service (C3S) Climate Data Store (CDS)*.
[36] E.-S. Im, J.S. Pal, E.A. Eltahir, Deadly heat waves projected in the densely populated agricultural regions of South Asia, Sci. Adv. 3 (8) (2017) e1603322.
[37] L. Inostroza, M. Palme, F. de la Barrera, A heat vulnerability index: spatial patterns of exposure, sensitivity and adaptive capacity for Santiago de Chile, PLoS One 11 (9) (2016) e0162464.
[38] IPCC, Climate Change 2021: The Physical Science Basis. Contribution of Working Group I to the Sixth Assessment Report of the Intergovernmental Panel on Climate Change, Cambridge University Press,, 2021.
[39] Jaxa. (2015). ALOS Global Digital Surface Model "ALOS World 3D–30m"(AW3D30). Retrieved from https://www.eorc.jaxa.jp/ALOS/en/dataset/aw3d30/aw3d30_e.htm. from Japan Aerospace Exploration Agency (JAXA) https://www.eorc.jaxa.jp/ALOS/en/dataset/aw3d30/aw3d30_e.htm.
[40] D.P. Johnson, et al., Developing an applied extreme heat vulnerability index utilizing socioeconomic and environmental data, Appl. Geogr. 35 (1-2) (2012) 23–31.
[41] J. Josse, F. Husson, Handling missing values in exploratory multivariate data analysis methods, J. De. la Société Fr. De. Stat. 153 (2) (2012) 79–99.
[42] J. Josse, F. Husson, missMDA: a package for handling missing values in multivariate data analysis, J. Stat. Softw. 70 (2016) 1–31.
[43] L.S. Kalkstein, et al., Increasing trees and high-albedo surfaces decreases heat impacts and mortality in Los Angeles, CA, Int. J. Biometeorol. 66 (5) (2022) 911–925.
[44] Karra, K., *et al.* , Global land use/land cover with Sentinel 2 and deep learning. ed. *2021 IEEE international geoscience and remote sensing symposium IGARSS*, 2021, 4704–4707.
[45] D.-W. Kim, et al., Mapping heatwave vulnerability in Korea, Nat. Hazards 89 (1) (2017) 35–55.
[46] H. Kim, D. Gu, H.Y. Kim, Effects of Urban Heat Island mitigation in various climate zones in the United States, Sustain. Cities Soc. 41 (2018) 841–852.
[47] R. Kotharkar, A. Ghosh, Review of heat wave studies and related urban policies in South Asia, Urban Clim., 36 (2021) 100777.
[48] R.S. Kovats, S. Hajat, Heat stress and public health: a critical review, Annu. Rev. Public Health 29 (2008) 41–55.
[49] Z. Liu, et al., Extracting the dynamics of urban expansion in China using DMSP-OLS nighttime light data from 1992 to 2008, Landsc. Urban Plan. 106 (1) (2012) 62–72.
[50] G. Luber, M. McGeehin, Climate change and extreme heat events, Am. J. Prev. Med. 35 (5) (2008) 429–435.
[51] Lyapustin, A., & Wang, Y. (2018). MCD19A2 MODIS/Terra+Aqua Land Aerosol Optical Depth Daily L2G Global 1km SIN Grid V006 [Data set] (Publication no. https://doi.org/10.5067/MODIS/MCD19A2.006). from NASA EOSDIS Land Processes DAAC.
[52] V.V.T. Mac, L.A. McCauley, Farmworker vulnerability to heat hazards: a conceptual framework, J. Nurs. Scholarsh. 49 (6) (2017) 617–624.

[53] G. Maier, et al., Assessing the performance of a vulnerability index during oppressive heat across Georgia, United States, Weather, Clim., Soc. 6 (2) (2014) 253–263.
[54] G. Manoli, et al., Magnitude of urban heat islands largely explained by climate and population, Nature 573 (7772) (2019) 55–60.
[55] B. Matsushita, et al., Sensitivity of the enhanced vegetation index (EVI) and normalized difference vegetation index (NDVI) to topographic effects: a case study in high-density cypress forest, Sensors 7 (11) (2007) 2636–2651.
[56] A.J. McMichael, et al., International study of temperature, heat and urban mortality: the 'ISOTHURM'project, Int. J. Epidemiol. 37 (5) (2008) 1121–1131.
[57] M. Moniruzzaman, et al., Decadal urban land use/land cover changes and its impact on surface runoff potential for the Dhaka City and surroundings using remote sensing, Remote Sens. 13 (1) (2020) 83.
[58] C. Mora, et al., Global risk of deadly heat, Nat. Clim. Change 7 (7) (2017) 501–506.
[59] M. Muhaimin, et al., Mapping build-up area density using normalized difference built-up index (ndbi) and urban index (ui) wetland in the city banjarmasin, in: IOP Conference Series: Earth and Environmental Science, 1089, IOP Publishing,, 2022 012036.
[60] T.D. Mushore, et al., Determining extreme heat vulnerability of Harare Metropolitan City using multispectral remote sensing and socio-economic data, J. Spat. Sci. 63 (1) (2018) 173–191.
[61] M.P. Naughton, et al., Heat-related mortality during a 1999 heat wave in Chicago, Am. J. Prev. Med. 22 (4) (2002) 221–227.
[62] J.E. Nichol, et al., Urban heat island diagnosis using ASTER satellite images and 'in situ'air temperature, Atmos. Res. 94 (2) (2009) 276–284.
[63] H. Nissan, et al., Defining and predicting heat waves in Bangladesh, J. Appl. Meteorol. Climatol. 56 (10) (2017) 2653–2670.
[64] H. Nissan, Á.G. Muñoz, S.J. Mason, Target. Model Eval. Clim. Serv.: a case Study Heat. Waves Bangladesh *Clim. Risk Manag.*, 28 (2020) 100213.
[65] Y. Niu, et al., A systematic review of the development and validation of the heat vulnerability index: major factors methods, and spatial units, Curr. Clim. Change Rep., 7 (3) (2021) 87–97.
[66] B.A. Norton, et al., Planning for cooler cities: a framework to prioritise green infrastructure to mitigate high temperatures in urban landscapes, Landsc. Urban Plan. 134 (2015) 127–138.
[67] M. Norusis, SPSS 12.0 statistical procedures companion. Upper Saddle, Prentice Hall,, NJ, 2003.
[68] J.A. Patz, et al., Impact of regional climate change on human health, Nature 438 (7066) (2005) 310–317.
[69] J. Podani, et al., Principal component analysis of incomplete data–A simple solution to an old problem, Ecol. Inform. 61 (2021) 101235.
[70] M. Poumadere, et al., The 2003 heat wave in France: dangerous climate change here and now, Risk Anal.: Int. J. 25 (6) (2005) 1483–1494.
[71] D.R. Raja, et al., Spatial distribution of heatwave vulnerability in a coastal city of Bangladesh, Environ. Chall. 4 (2021) 100122.
[72] J. Refslund, et al., Development of satellite green vegetation fraction time series for use in mesoscale modeling: application to the European heat wave 2006, Theor. Appl. Climatol. 117 (2014) 377–392.
[73] C. Rinner, et al., The role of maps in neighborhood-level heat vulnerability assessment for the city of Toronto, Cartogr. Geogr. Inf. Sci. 37 (1) (2010) 31–44.
[74] S. Roy, et al., Examining the nexus between land surface temperature and urban growth in Chattogram Metropolitan Area of Bangladesh using long term Landsat series data, Urban Clim. 32 (2020) 100593.
[75] D.B. Rubin, Multiple imputation for nonresponse in surveys, John Wiley & Sons,, 2004.
[76] Salvati, A. and Kolokotroni, M. 2020. Impact of urban albedo on microclimate and thermal comfort over a heat wave event in London.
[77] S. Saneinejad, P. Moonen, J. Carmeliet, Comparative assessment of various heat island mitigation measures, Build. Environ. 73 (2014) 162–170.
[78] Schaaf, C., & Wang, Z. (2015). MCD43A3 MODIS/Terra+Aqua BRDF/Albedo Daily L3 Global - 500m V006 [Data set] (Publication no. https://doi.org/10.5067/MODIS/MCD43A3.006). from NASA EOSDIS Land Processes DAAC.
[79] M.C. Schmidtlein, et al., A sensitivity analysis of the social vulnerability index, Risk Anal.: Int. J. 28 (4) (2008) 1099–1114.
[80] A. Sharma, G. Andhikaputra, Y.-C. Wang, Heatwaves in South Asia: characterization, consequences on human health, and adaptation strategies, Atmosphere 13 (5) (2022) 734.
[81] S.C. Sheridan, M.J. Allen, Temporal trends in human vulnerability to excessive heat, Environ. Res. Lett. 13 (4) (2018) 043001.
[82] J.E. Steele, et al., Mapping poverty using mobile phone and satellite data, J. R. Soc. Interface 14 (127) (2017) 20160690.
[83] S. Tawsif, M.S. Alam, A. Al-Maruf, How households adapt to heat wave for livable habitat? A case of medium-sized city in Bangladesh, Surrent Res. Environ. Sustain. 4 (2022) 100159.
[84] C.K. Uejio, et al., Intra-urban societal vulnerability to extreme heat: the role of heat exposure and the built environment, socioeconomics, and neighborhood stability, Health Place 17 (2) (2011) 498–507.
[85] I. Ullah, et al., Projected changes in socioeconomic exposure to heatwaves in South Asia under changing climate, Earth'S. Future 10 (2) (2022) e2021EF002240.
[86] S. Ullah, et al., Future population exposure to daytime and nighttime heat waves in South Asia, Earth'S. Future 10 (5) (2022) e2021EF002511.
[87] Z. Wan, New refinements and validation of the collection-6 MODIS land-surface temperature/emissivity product, Remote Sens. Environ. 140 (2014) 36–45.
[88] Wan, Z., Hook, S., & Hulley, G. (2015). MOD11A2 MODIS/Terra Land Surface Temperature/Emissivity 8-Day L3 Global 1km SIN Grid V006 [Data set] (Publication no. https://doi.org/10.5067/MODIS/MOD11A2.006). from NASA EOSDIS Land Processes DAAC.
[89] Y.-R. Wang, et al., Evaluating global and regional land warming trends in the past decades with both MODIS and ERA5-Land land surface temperature data, Remote Sens. Environ. 280 (2022) 113181.
[90] B.W. Wheeler, et al., Beyond greenspace: an ecological study of population general health and indicators of natural environment type and quality, Int. J. Health Geogr. 14 (1) (2015) 1–17.
[91] T. Wolf, G. McGregor, The development of a heat wave vulnerability index for London, U. Kingd. Weather Clim. Extrem., 1 (2013) 59–68.
[92] WorldPop. (2018). Global High Resolution Population Denominators Project - Funded by The Bill and Melinda Gates Foundation (OPP1134076) (Publication no. https://doi.org/10.5258/SOTON/WP00645).
[93] Y. Xiang, et al., Seasonal variations for combined effects of landscape metrics on land surface temperature (LST) and aerosol optical depth (AOD), Ecol. Indic. 138 (2022) 108810.
[94] J. Yang, et al., Heatwave and mortality in 31 major Chinese cities: definition, vulnerability and implications, Sci. Total Environ. 649 (2019) 695–702.
[95] W. Zhang, P. McManus, E. Duncan, A raster-based subdividing indicator to map urban heat vulnerability: a case study in sydney, australia, Int. J. Environ. Res. Public Health 15 (11) (2018) 2516.
[96] L. Zhao, et al., Interactions between urban heat islands and heat waves, Environ. Res. Lett. 13 (3) (2018) 034003.
[97] S.S. Zuhra, A.B. Tabinda, A. Yasar, Appraisal of the heat vulnerability index in Punjab: a case study of spatial pattern for exposure, sensitivity, and adaptive capacity in megacity Lahore, Pakistan, Int. J. Biometeorol. 63 (12) (2019) 1669–1682.